UNIVERSITY OF CALIFORNIA, SAN DIEGO

Water Transport And Homeostasis: The Third Major Function of Erythrocytes

A Dissertation submitted in partial satisfaction of the requirements
for the degree Doctor of Philosophy

in

Bioengineering

by

Joseph Sugie

Committee in charge:

Professor Lanping Amy Sung, Chair
Professor Marcos Intaglietta, Co-Chair
Professor Kim Barrett
Professor Ju Chen
Professor Geert Schmid-Schönbein

2016

The Dissertation of Joseph Sugie is approved, and it is acceptable in quality and form for publication on microfilm and electronically:

Co-Chair

Chair

University of California, San Diego

2016

DEDICATION

To my family and friends,

Thank you for the love, support and guidance.

EPIGRAPH

…"Is the model true?" If "truth" is to be the "whole truth" the answer must be "No".

The only question of interest is "is the model illuminating and useful?"

– George Box

TABLE OF CONTENTS

LIST OF ABBREVIATIONS

2D	Two dimensional
3D	Three dimensional
AQP	Aquaporin
AQP1	Aquaporin-1
C	Celsius
CA	California
CHIP28	Channel forming integral membrane protein of relative mass 28
Cl	Chloride
cm	centimeter
DAB	3-3’ Diaminobenzidene
g	gram
IMOD	Image processing modeling and display tools
K	Potassium
KO	Knock out
L	Liter
mL	milliliter
mm	millimeter
mm	micrometer
nm	nanometer
mRNA	messenger ribonucleic acid
SDS-PAGE	sodium dodecyl sulfate polyacrylamide gel electrophoresis
mOsM	milliosmolar
Na	Sodium
OCT	Optimum cutting temperature compound
PBS	Phosphate buffered saline
PDMS	Polydimethylsiloxane
fL	femtoliter
RBC	Red blood cell/erythrocytes
s	second
WT	Wild-type
µL	microliter

LIST OF FIGURES

LIST OF TABLES

ACKNOWLEDGEMENTS

First and foremost I would like to thank my advisor Dr. Lanping Amy Sung for the inspiration and continued guidance that she provided. The direction through long edits of multiple drafts has been invaluable.

I would also like to acknowledge my co-chair Dr. Marcos Intaglietta for his detailed discussions with me and the knowledge that his door was always open. In addition, I would like to thank my committee members for their continued support, optimism and advice.

I would also like to acknowledge my roommates. During this trying time, they have kept me level headed and provided assistance whenever possible.

Additionally, I would like to thank Ryan Johnson from the Hasty lab who served as a mentor for the production of my microfluidic chip.

Chapters 1, 2 and 3, in part are currently being prepared for submission for publication of the material. Sugie, Joseph; Sung, L. Amy. The dissertation author was the primary investigator and author of this material.

VITA

2006-2009	Provost's Honors, University of California, San Diego
2008-2010	Undergraduate Researcher, Department of Nanoengineering, University of California, San Diego
2010	Bachelor of Science, Department of Bioengineering, University of California, San Diego
2010-2011	Teaching Assistant, Department of Bioengineering, University of California, San Diego
2011-2012	Teaching Assistant, Department of Bioengineering, University of California, San Diego
2012	Master of Science, Department of Bioengineering, University of California, San Diego
2013-2014	Teaching Assistant, Department of Bioengineering, University of California, San Diego
2014-2015	Teaching Assistant, Department of Bioengineering, University of California, San Diego
2016	Doctor of Philosophy, Department of Bioengineering, University of California, San Diego

ABSTRACT OF THE DISSERTATION

Water Transport and Homeostasis:
The Third Major Function of Erythrocytes

by

Joseph Sugie

Doctor of Philosophy in Bioengineering

University of California, San Diego, 2016

Professor Lanping Amy Sung, Chair

Professor Marcos Intaglietta, Co-Chair

Aquaporin-1 (AQP1) was first identified in the red blood cell as an abundant transmembrane water channel protein in 1992. It is also expressed in the brain, lung, eye and kidney. However, since the initial discovery and subsequent characterization of molecular structure, the physiological role of AQP1 in the red blood cell has not been fully understood.

We propose red blood cells with AQP1 act as regulators of local osmolarity and water homeostasis based on their capacity for volume change, rapid water transport, mobility and presence throughout the body. Firstly, use of a newly developed negative imaging technique along with confocal microscopy enabled large scale *in vivo* data collection and measurement necessary to explore red blood cell volume distributions in mouse kidneys. These results revealed the volume capacity of normal red blood cells showing a gradual decrease up to 40% in response to the presumed hyperosmotic gradient within the medulla. In contrast, AQP1 knockout (KO) cells displayed minimal reduction of volumes. Secondly, in continuation and expansion of these results, Kedem-Katchalsky equations of membrane transport were used to model normal and AQP1 KO systems beyond *in vivo* or *in vitro* experiments. The fast water transport coupled with cell volume changes enables erythrocytes to function as “micropumps” to facilitate osmolarity regulation. Simulations also uncovered the role red blood cells play in the osmotic gradient established by the countercurrent multiplier of the kidney. Thirdly, a microfluidic device was designed and constructed to measure the sensitive kinetics of normal and AQP1 KO red blood cells *in vitro* in conditions resembling capillary flow conditions. Testing this system against various hypotonic and hypertonic conditions with a fluorescent indicator present in the extracellular compartment revealed that exchanges between normal red blood cells and their surroundings were capable of reaching steady-state in 60 ms.

Combining experimental results and theoretical analyses allows for greater insight in our understanding of the role red blood cells played in water balance. Thus, in addition to both O_2 and CO_2 exchanges, we propose water transport and homeostasis may be the third major function of red blood cells.

INTRODUCTION

There are approximately 20-30 trillion red blood cells circulating in our body. Their two major well established functions are O_2 and CO_2 exchanges. While O_2 exchange occurs by diffusion across the lipid bilayer of the cell membrane, the CO_2 exchange is facilitated by its conversion to HCO_3^- and the action of anion exchanger, an integral membrane protein in the erythrocyte membrane. Without these exchanges, individuals are only able to survive for a few minutes.

Seventy percent (70%) of human bodies are made out of water. Without the uptake of water, individuals are not able to live for more than a few days. The relatively short period of time, compared to two weeks of survival time after food deprivation, demonstrates the importance of uptake and homeostasis of water. The functional role of red blood cells, which express 200,000 water channel proteins, in water transport and homeostasis deserved to be investigated.

The erythrocyte membrane proteins have been extensively studied since techniques like SDS-polyacrylamide gel electrophoresis (SDS-PAGE) in the 1970s and molecular biology in the 1980s were used. About a dozen or more major and minor membrane protein bands can be identified by SDS-PAGE. Several membrane proteins co-migrate as band 7. CHIP28 (CHannel forming Integral membrane Protein of relative mass 28 kDa) was first identified as one of the proteins in band 7 of human erythrocyte membrane by Agre and his colleagues in 1992 [Preston et al. 1992]. To confirm the suspicion that it may be a channel protein, *in vitro* transcribed RNA coding for the human CHIP28 was microinjected and expressed in Xenopus oocytes. When the oocytes (which do not normally express water channels) were immersed in hypotonic 70 mOsM solution, they rapidly swelled and exploded due to an influx of water. The first water channel was thus discovered, and the protein was renamed aquaporin. With the subsequent

discovery of many CHIP28 homologs, it was revealed that there is a broad family of water channels. Peter Agre was later awarded the 2003 Nobel Prize in Chemistry for his discovery of aquaporins.

The specificity of water channels has been well studied by X-ray crystallography. Structural analysis revealed that each monomer of the homotetrameric AQP1 (the aquaporin in red blood cells) contains a highly specific water channel with a selectivity filter consisting of an aromatic and arginine residue [Walz et al., 1997, Kosinska et al., 2013]. The mechanisms by which the water molecules are aligned in a specific orientation, and the transfer of protons through the channel is prevented have been revealed for AQP1. Different aquaporins vary in their specificity for water and thirteen human variants of aquaporin have been found [Verkman, A.S. 2005].

Reviewing cellular and molecular biology of the aquaporin water channels suggests that AQP1 may be a constitutively active, unregulated water channel allowing water transport in the direction of higher osmotic strength [Borgnia et al., 1999]. The complete regulation of AQP1 in various cell types or tissues is not fully understood [Nielsen et al., 2002]. However, recent studies on reticulocytes have revealed a reduction of AQP1 by exosomal sorting (pinching off membrane pieces containing AQP1) in response to increasing tonicity of the external medium which implies regulation by extracellular osmotic conditions prior to maturation [Blanc et al., 2009]. In addition, for cholangiocytes, the epithelial cells of the bile duct, the localization of AQP1 was reported to change from the cytoplasm to the plasma membrane in response to stimulation with secretin [Nielsen et al., 1993; Carbrey, J.M and Agre, P. 2009].

Measurements of osmotic water permeability of red blood cells have demonstrated the ability of AQP1 to transport water rapidly. Light scattering experiments utilizing a 100 mM inwardly directed sucrose gradient comparing wild-type mice to AQP1 KO mice showed a decrease in osmotic water permeability from 0.018 cm/s to less than 0.003 cm/s [Yang, B., Ma, T., and Verkman, A.S. 2001]. In comparison, the permeability of a lipid bilayer for water is typically within the range of 0.23-63 μm/s [Thompson, T.E., and Huang, C., 1966]. These studies suggest that AQP1 is the major contributor to the water permeability of the erythrocyte membrane.

AQP1 is known to express in several other tissues including the eye, the lungs, the brain and the kidney [King, L., Yasui, M., and Agre, P., 2000; Effros et al., 1997; Nielsen et al., 2000]. In the kidney, AQP1 is found in the proximal tubule, the thin descending limb of the loop of Henle, and the endothelial cells of the capillary network associated with the loop of Henle termed the vasa recta. These tissues are known contributing factors critical to the production of urine within the kidney. AQP1 knockout mice are unable to concentrate urine and suffer from polyuria indicating the importance of AQP1 in the regulation of water transport and homeostasis in the kidney [Ma et al., 1998]. As a result of impaired kidney function, the AQP1 knockout mice generally display elevated serum osmolarity compared to wild-type mice. Similar findings have also been reported in human patients [Gregory et al., 1994].

The functional roll of AQP1 in red blood cells in vasa recta and other tissues, however, is not fully understood, despite having 200,000 copies per cell in the membrane [King et al. 2000]. Because AQP1 is found in several cell types in non-

erythroid tissues, and there exists no cell specific promoter to create erythrocyte-specific knockout model, the function of AQP1 in erythrocytes is difficult to study.

Despite over two decades of research on aquaporins since their discovery and characterization, the function of AQP1 in the erythrocyte membrane has not been fully understood. We suggest that rapid water transport in the red blood cell allows it to function as a regulator of local osmolarity, and given the presence of erythrocytes throughout the body in circulation they may contribute to water homeostasis.

This suggestion was based on several properties of the red blood cell which make it a good candidate for a regulator. The large number of red blood cells present throughout the body at all times, combined with the volume of blood they occupy indicates a potentially significant amount of water capable of transport. Additionally, each red blood cell is capable of volume change in response to osmotic pressure, suggesting an ability to store excess or release extra water. Most critically, the presence of 200,000 AQP1 within the membrane allow for water to both enter and release rapidly. In order for this hypothesis to be feasible, (1) red blood cells need to be able to *rapidly* transport water *in vivo* in response to osmotic stress, and (2) the amount of water transport needs to be *large* enough to affect the surrounding plasma in a meaningful way.

In Chapter 1, the ability of red blood cells to exchange water locally in the capillaries of vasa recta in response to the changing osmolarity gradient of the kidney *in vivo* was investigated. In Chapter 2, a computational model of water transport among 3 compartments (*i.e*., erythrocyte, plasma, and interstitial fluid) was developed to show a regulatory function of erythrocytes as a result of rapid response to the osmotic gradient. In chapter 3, a microfluid device was designed

and manufactured to measure the timescale and magnitude of erythrocytes' response to extracellular (resembling plasma) osmolarity, demonstrating erythrocytes' regulatory effects in an *in vitro* system.

CHAPTER 1

In Vivo Response of Erythrocytes to Osmotic Gradients in Renal Capillaries

Introduction

In vitro measurements of red blood cell permeability to water made by the Agre lab and the Verkman lab suggest that water transport occurs on a millisecond timescale [Yang et al., 2001; Carbrey, J. and Agre, P., 2009] . In order to observe red blood cell volume changes *in vivo*, a natural osmotic gradient in tissues is required. The tissue adjacent to the loop of Henle within the kidney provides a directional gradient from isosmotic conditions of 300 mOsM to as much as approximately 1200 mOsM or higher [Gottschalk, C.W. and Mylle, M., 1959]. The capillaries in this tissue are referred to as the vasa recta and typically run in parallel to the loop of Henle, branching or terminating at points along the loop to form a mesh-like network.

The extent of the volume changes of erythrocytes in these capillaries should give an indication as to the effective water permeability *in vivo*. Each functional unit (nephron) of the kidney has a pyramidal shape and similar, relative orientation. In general, a position farther from the cortex and closer to the center of the medulla will have higher osmolarity. In practice, the directionality of the loop of Henle provides an easy way to track and approximate changing osmolarity. When averaged over many measurements, this general trend should persist despite variable lengths of individual tubules or loops.

High osmolarity in the medulla of the kidney is primarily a result of the countercurrent mechanism for the concentration of urine by the loop of Henle. The conventional explanation begins with sodium, potassium and chloride (by $Na/K/Cl_2$ pumps) in the thick ascending limb which is actively pumped out into the surrounding tissue causing passive transport of water out from the descending limb [Gottschalk, C.W. and Mylle, M., 1958]. The presence of AQP1 in the descending

limb allows for the continuous loss of water to hyperosmotic surroundings as filtrate progresses down the loop of Henle [Nielsen et al., 2001]. As a result, the filtrate becomes increasing concentrated towards the inner medulla. While this is often the most cited explanation for urine concentration, several new hypotheses have arisen amid concerns of the energy balance involved in continuous active pumping of salts. Newer explanations for urine concentrations have been made proposing a lack of active transport altogether [Kokko, J.P. and Rector, F.C., 1972].

However, more recent studies have indicated that details of this mechanism are still unexplained despite decades of sustained research [Layton et al., 2004]. While the exact details for the generation of the gradient are not absolutely conclusive, the original micropuncture experiments made in 1959 measuring the osmolarity in the medulla are not in dispute.

In close proximity to the loop of Henle is the associated capillary network termed the vasa recta (Latin for straight vessels). Capillaries within this network run adjacent to the loop of Henle and are exposed to higher osmolarity found within the interstitial fluid of the medulla. Red blood cells passing through the vasa recta experience hyperosmotic conditions *in vivo* making the kidney ideal for studying their physiological response to an elevated osmolarity gradient. Studies on AQP1 knockout mouse models thus far have focused on the obvious disease states, polyuria and a decreased ability to concentrate urine. These effects are a direct result of decreased water transport in kidney tissues. Because AQP1 is present in renal tissues in addition to red blood cells, it is difficult to elucidate the function of the water channel in only these cells. A tissue specific promoter for red blood cells does not exist which means the effects of both kidney tissue and red blood cells must be considered when examining an AQP1 knockout mouse model.

The proposed function of red blood cell water transport is as a local regulator of osmolarity and as such, impaired function would create an inability to handle fluctuations of salt concentrations. Given the presence of AQP1 in the kidney, the role of rapid water transport in red blood cells would be difficult to separate from the effect due to the loss of proper kidney function. To observe whether or not red blood cells can respond to a naturally maintained osmolarity gradient *in vivo*, volume measurements of red blood cells throughout the kidney were obtained. Using confocal microscopy to image large sections of the kidney at multiple depths provides the data necessary to complete a 3D reconstruction of the tissue and the red blood cells. Tissue sections stained with 3, 3'-Diaminobenzidine (DAB) and mounted with media containing the fluorescent dye ATTO 655 provide enough contrast between red blood cells and surrounding tissue to generate consistent 3D models. By comparing red blood cell volumes from wild type mice to those from AQP1 knockouts, the overall effect of the water channel can be visualized.

Methods

Kidney and tissue preparation

Wild-type (WT) mice with a background of C57/Black and 129/Svj between 6 months and 18 months were sacrificed via cervical dislocation and kidneys were removed by excision within 15 seconds. To compare blood loss effects, renal arteries and veins were tied off prior to excision. Immediate immersion in fixative occurred post excision to prevent any changes to red blood cell morphology due to blood loss in the kidney. Kidneys were placed in 4% paraformaldehyde and incubated at 4 °C for 12-24 hours. Kidneys were then transferred to a 30% sucrose

solution at 4 °C for 24-48 hours. Following cryoprotection with sucrose, kidneys were embedded in OCT (Tissue-tek Optimum Cutting Temperature compound, SAKURA FINETEK USA INC, Torrence, CA) and frozen using dry ice. Embedded kidneys were stored at -20 °C until sectioned via cryostat. Kidneys from 3 male and 2 female WT mice as well as 2 male and 1 female KO mice were used for subsequent red blood cell volume measurements. Preparation of 4% paraformaldehyde occurred as follows. 150 mL of 1X PBS was added to a PYREX 250 mL Erlenmeyer flask and placed in a 500 mL beaker containing 100 mL of deionized water. The beaker was placed on a hotplate and heated to 58 °C. After reaching temperature, 4 g of paraformaldehyde powder was added to the heated PBS and stirred until dissolved. Solution was filtered once clear and made into 50 mL aliquots for storage at -20° Celsius. Before use, paraformaldehyde solutions was placed in a water bath at 37° C until thawed and then transferred to 4° C for 30 minutes before use.

Kidney staining and mounting

Mouse kidneys were sectioned via cryostat while embedded in OCT at a temperature of -20° Celsius. Sections of 20-30 µm kidney tissue on glass slides were washed with deionized water 5 times to remove traces of OCT. Excess water was removed from the slide and 20 µL of 10% hydrogen peroxide was added directly on top of each section for 10 minutes. Slides were washed 3 times in deionized water to remove any remaining hydrogen peroxide and excess water was removed from the slide. Each slide is covered in a working solution of DAB (from Innovex biosciences) and incubated for 5 minutes. Slides were washed 5 times with deionized water before air drying for 5 minutes. Counterstaining was

accomplished using 20 µL of a 1:100 diluted ATTO 655 (Sigma-Aldrich, St. Louis, MO) stock solution is used to mount each slide with a #1.5 glass coverslip. Slides were imaged within 8 hours of preparation.

Confocal microscopy

Imaging occurred on an Olympus FV1000 Spectral Confocal microscope in the UCSD Neuroscience/Microscopy Core. Image stacks were obtained with a *z*-spacing of 0.2 microns for the entire section resulting in 100-150 images per stack. Images were taken with 1024 x 1024 resolution resulting in a 0.0308 µm/pixel ratio. Image *x/y* locations were taken relative to each other and with the directionality of the loop of Henle in mind.

3D reconstruction

Image stacks obtained through microscopy were processed through IMOD to obtain volumetric meshes from each cell. Selected images from each stack were chosen as seed images and contours were generated around each red blood cell in the image. Contours from seed images were used to automatically generate contours around cells in each intermediary image. The resulting meshes were composed of data with a resolution of 0.2 µm in the *z*-direction and 0.0308 µm in the *x/y*-direction. Volume of each mesh was calculated as a linear approximation of a 3D volume from the combined 2D surface contours.

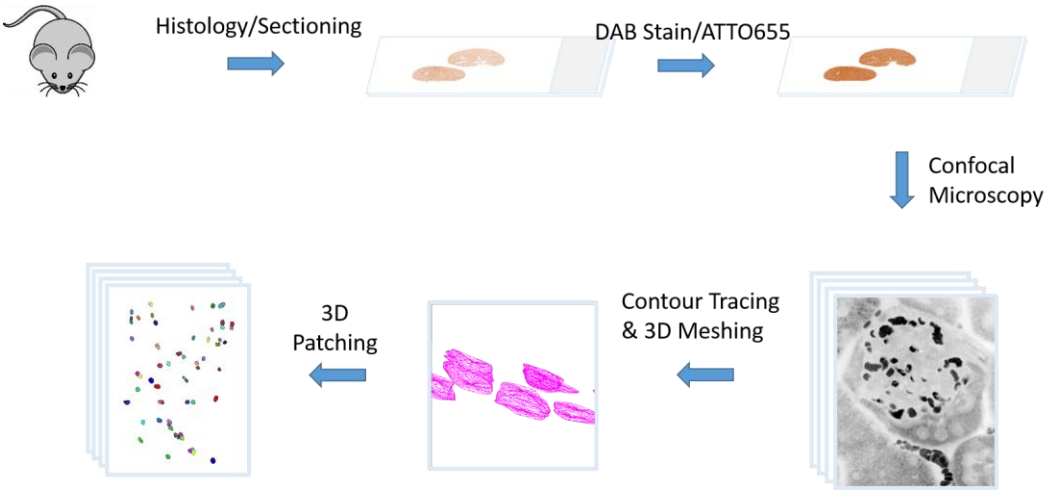

Figure 1.1 Overview of chapter 1 methods for 3D reconstruction of red blood cells. Following histology of mice kidneys, negative imaging is accomplished with DAB and ATTO 655. Image stacks obtained from confocal imaging are processed using IMOD to create 3D reconstructions of red blood cells.

Results

Viability of DAB staining

The chemical compound 3, 3'-diaminobenzidene (DAB) reacts with peroxidase activity to produce a dark brown non-soluble deposit. By removing all other endogenous peroxidase activity in kidney sections with excess hydrogen peroxide (see Methods), DAB only stained red blood cells. Kidney tissue naturally exhibits low levels of fluorescence however the lumen of the tubule system and blood vessels would not be capable of producing a signal using confocal microscopy without the presence of a fluorophore. By mounting kidney tissues using a low concentration of ATTO 655, fluorescent signals can be generated from everything in the background except the DAB stained red blood cells. This negative staining technique developed in this thesis enabled the accurate construction of contours for all erythrocytes within the imaged field of view.

Figure 1.2 demonstrates the ability of DAB and ATTO 655 to provide enough contrast to easily distinguish individual red blood cells. Even at low magnifications, contrast was high enough to distinguish individual red blood cells. Even in single images, cell border detection is complicated by the often close proximity exhibited by red blood cells. Comparison of Figure 1.2A and 1.2B reveals the advantage of confocal microscopy over traditional fluorescent microscopy Red blood cells are prone to overlap when imaging thick 30 μm sections, creating large DAB stained sections barely distinguishable as clumps of cells. By focusing on a single plane, such overlaps become impossible, creating the assurance that each separate DAB stain is an individual red blood cell. While the complete red blood cell is captured in a traditional fluorescent image, a more useful slice is obtained with confocal microscopy.

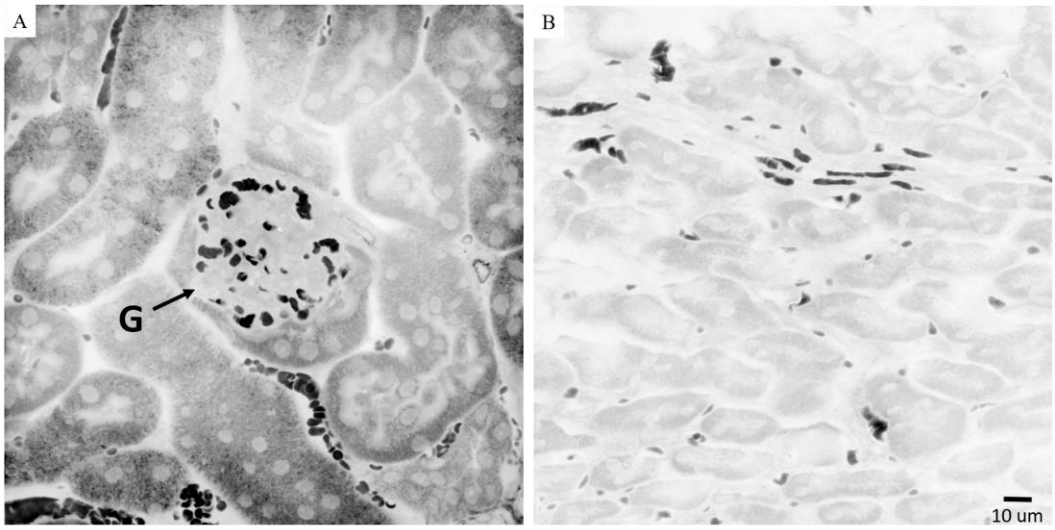

Figure 1.2 Mouse kidney sections stained with 3, 3'-diaminobenzidene. Sections 30 micron thick stained with DAB and counterstained with ATTO 655 demonstrate the high contrast and sharp red blood cell profiles that can be obtained. Red blood cells in both glomeruli (A) and capillaries (B) are clearly seen as dark spots in this negative imaging method.

The pyramidal shape of the nephron is often not as clear as illustrations would suggest. Figure 1.3 shows a real example of this shape. The transition from cortex to medulla is most visibly marked by the lack of glomeruli and the appearance of striations, caused by long loops of Henle and capillaries that denote the axially directed osmotic gradient. Notably, the presence of ATTO 655 fluorescent dye serves to help distinguish cortex from medulla by localizing more in the latter due to the increased presence of tubules. Higher endothelial cell density and the presence of glomeruli in the cortex contribute to a lower fluorescent signal compared to the medulla. In order to compare data taken from multiple sequential sections or multiple kidneys, the direction of the medulla was identified and used to scale the data to the axis of the osmotic gradient.

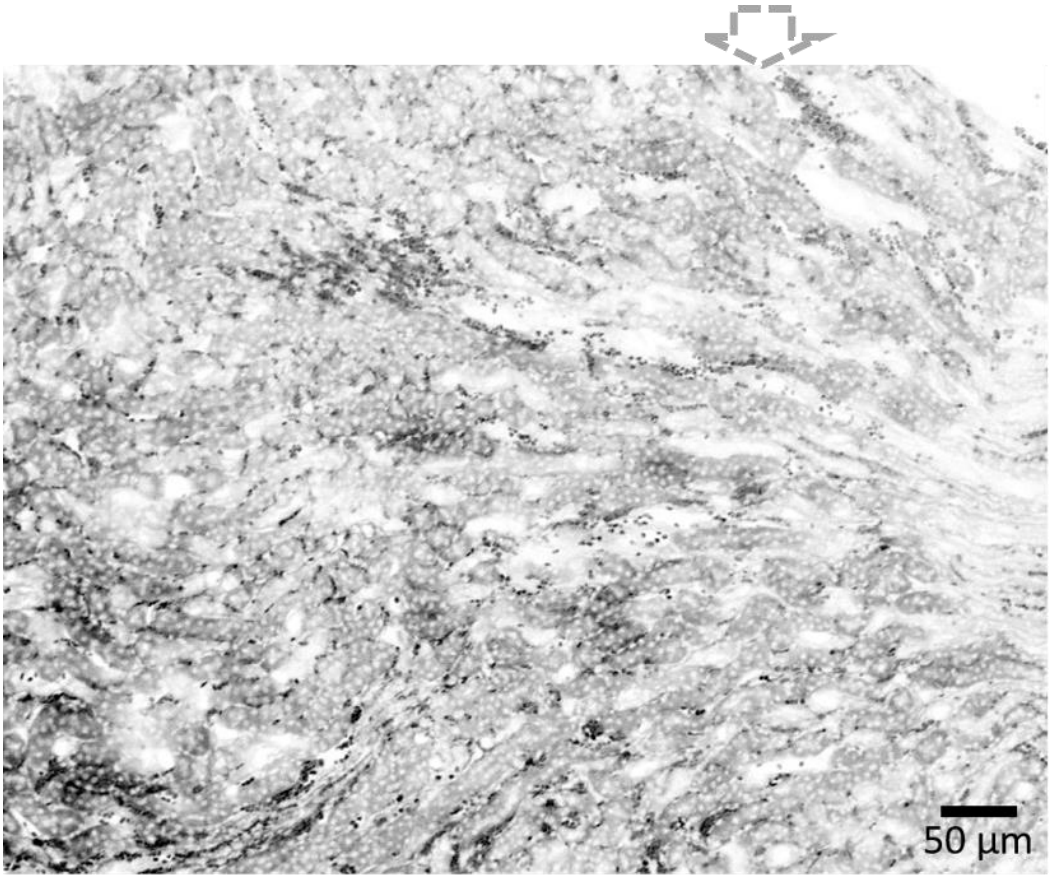

Figure 1.3 Low magnification view of mouse kidney section stained with DAB. Black dots on are individual red blood cells stained with DAB. Cortex can be seen on to the left and medulla to the right. A broad arrow indicates the border. Presence of glomeruli in the cortex clumps together many red blood cells giving the cortex a darker appearance overall with more dark spots.

Contouring and 3D meshing

The result of meshing for a set of red blood cell contours can be visualized through OpenGL as in Figure 1.4. Individual contours from each image in a stack were connected to form 3D objects. The accuracy of the meshing depends on the accuracy of the contour, the z-direction resolution of the image stack, the consistency of the imaging conditions as well as the resolution of the contours themselves.

Meshes are capped assuming the beginning and ending contours are flat objects which is incorrect but the only way to ensure consistency. Depending on the position of the red blood cell relative to the imaging surface the size of the red blood cell cross section changes. In general, larger cross sections would be affected more by flat capping as a larger surface is being approximated. The effect of this is more pronounced in highly rounded cells and particularly in cells which have a large final contour. Triangular meshing between contours is a form of linear approximation. With high contour resolution, good approximations of complex surfaces can be made.

Red blood cell volume distributions and histograms

Figure 1.5 shows the distribution of red blood cell volumes in 3D space. This representation of red blood cell volumes reveals a distribution of sizes at any given depth in the medulla. In C57/Black mice, the average red blood cell size is 50 fL. Cells of this size are mainly found towards the cortex in all samples. By arranging volumetric data along the axis from cortex to medulla, a decreasing trend becomes apparent. Average red blood cell volume is higher in the cortex than in the medulla.

Comparing wild type and AQP1 knockout volume distributions reveals a much greater variance in volume sizes in the wild type (Figure 1.6). Additionally, no trend in directionality is immediately apparent from the AQP1 knockout red blood cells. The overall lack of volume change is an expected result based on the decreased water permeability of the erythrocyte membrane as well as an impaired urine concentrating mechanism found in the AQP1 mouse model [Ma et al., 1998].

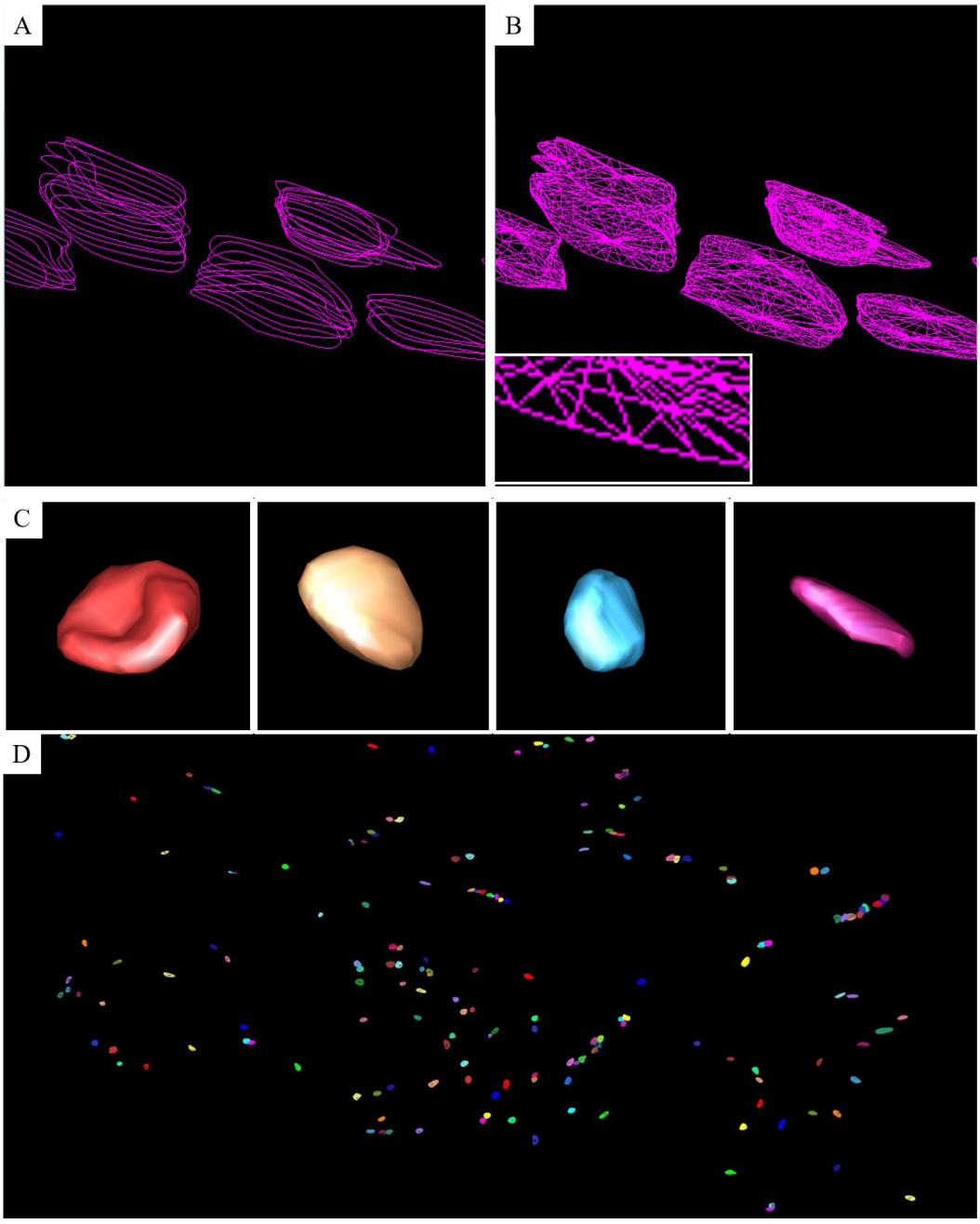

Figure 1.4 Contours and 3D meshes made from red blood cells imaged through confocal microscopy. (A) Contours made around cells from a single image were combined with contours from the image stack. (B) Triangular meshing with IMOD was used to connect the contours and form complete 3D objects. (C) Representative blood cells shown from cortex with normal morphology and vasa recta capillaries with smaller deformed or elongated forms. (D) All meshed red blood cells from a single kidney section visualized in Open Graphics Library (OpenGL) with false color to distinguish individual cells.

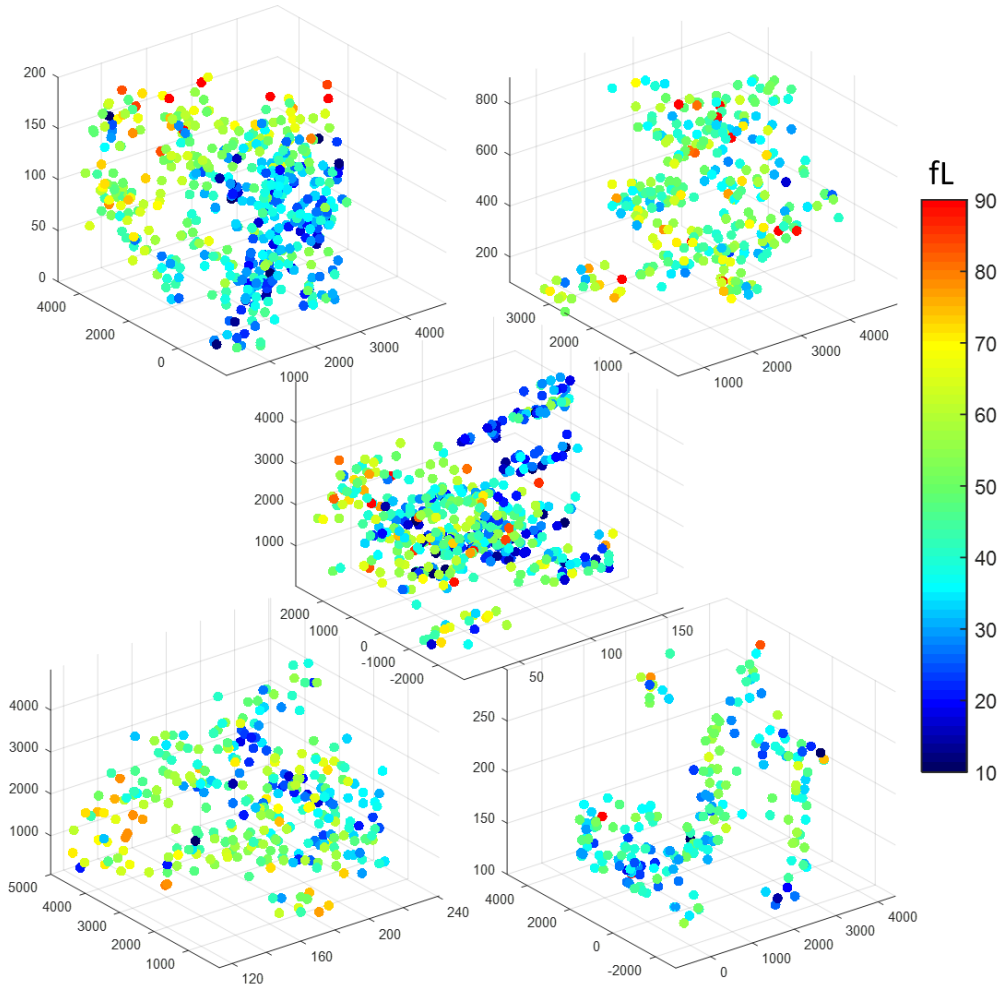

Figure 1.5 Color maps of red blood cell volume distribution in wild-type mouse kidneys. Five maps showing the volume distributions for 5 mouse kidneys (3 male, 2 female) arranged with cortex facing left and medulla facing right. Mean erythrocyte volume for a C57B/6 mouse is 50 fL (green). Smaller than average cells were typically seen in the medulla. (Enlarged maps for individual kidneys and their histograms are provided in the supplementary figures).

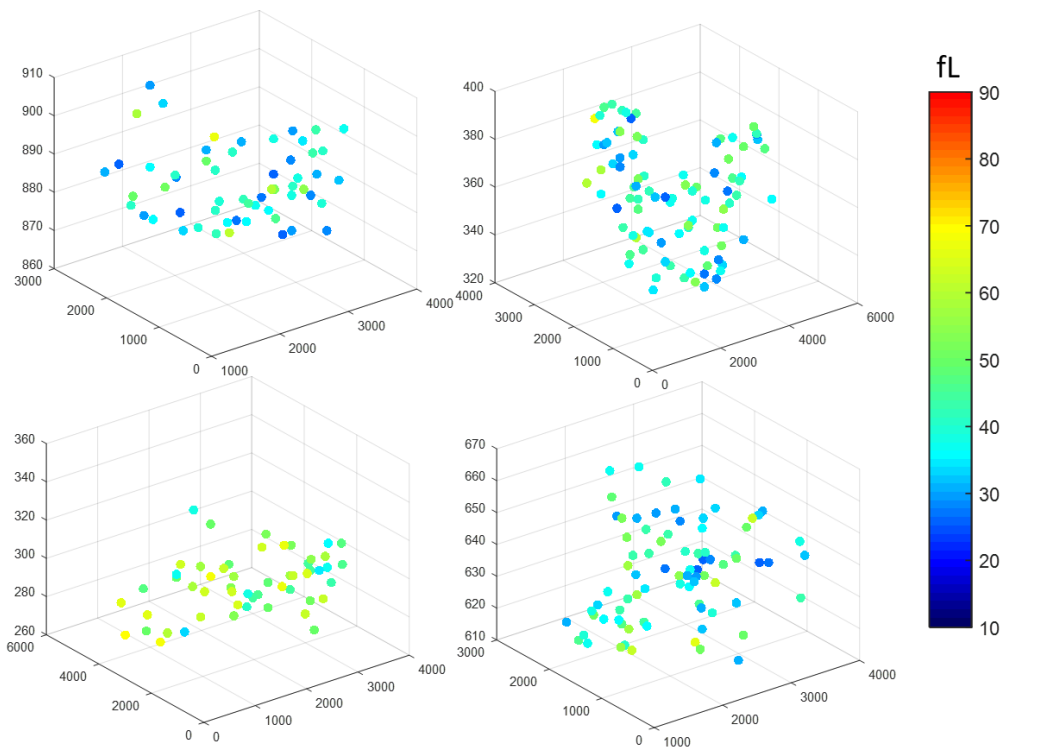

Figure 1.6 Color maps of red blood cell distribution in AQP1 KO mouse kidneys. Volume distributions for 4 mouse kidneys (2 male, 2 female) arranged with cortex facing left and medulla facing right. Less variance in volume is seen with AQP1 knockout when compared with wild type. (Enlarged maps for individual kidneys and their histograms are provided in the supplementary figures).

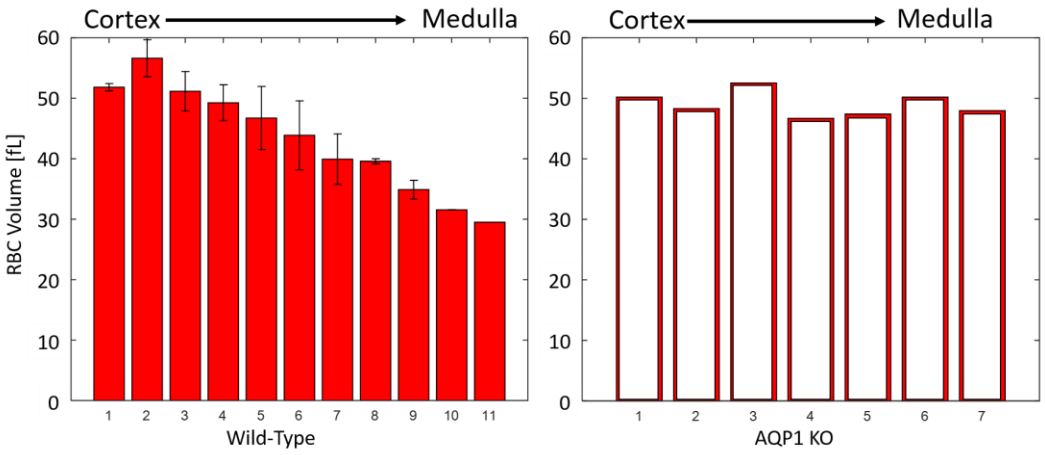

Figure 1.7 Histogram of red blood cell volume data oriented in the direction of the osmotic gradient in the kidney. Wild type mouse red blood cells show a decrease of approximately 40% from cortex to medulla. Over a similar distance, no perceptible change is observed in the AQP1 knockout red blood cells.

Histograms in Figure 1.7 of the volume data oriented in the direction of the osmotic gradient show a general trend of decreasing red blood cell volume corresponding to the increase in osmolarity in the medulla. The larger error bars for data from the outer medulla indicates a wider distribution of red blood cell volumes. A few kidneys showed an increase in red blood cell volume close to the cortex which is consistent with the hypotonic conditions present on the venous side of the vasa recta [Gottschalk, C.W. and Mylle, M., 1959]. In the inner medulla, assumed to be the highest osmolarity, the red blood cells revealed a 40% decrease compared to the volume of the cells within the cortex and large arteries. In comparison, the AQP1 knockouts showed relatively small volume change. While there were individual cells that exhibited smaller volumes, the overall trend displayed no real change moving from cortex to medulla. In combined histograms for the wild type, each individual bar contains data from over a hundred red blood cells and the large changes observed are statistically significant when compared to the knockout.

Discussion

Red blood cell volume distribution

Histograms of the data from wild-type and AQP1 knockout mice reveal a distinct difference in red blood cell volumes within the medulla. However whether this effect is entirely due to the lack of AQP1 in the erythrocyte membrane is unclear. AQP1 has many functions and is present in multiple tissues throughout the body including the vasa recta. One of the hypothesized functions of AQP1 in the kidney is towards the generation of the osmotic gradient and AQP1 knockouts lack the ability to concentrate urine. This would indicate that the observed

difference is a compound of two effects; namely, the decrease in permeability of the erythrocyte membrane as well as the decrease in magnitude of the osmotic gradient in the medulla. Because no tissue specific markers exist for mature red blood cells, a targeted knockout of AQP1 in red blood cells is unlikely thus far and the individual effect of AQP1 in the erythrocyte membrane is difficult to detangle *in vivo*.

However, the difference in response between wild-type and AQP1 knockout red blood cells does indicate that the decreasing trend observed in the wild-type cells is not an artifact of the sample preparation. Efforts are made during tissue collection to minimize blood loss and prevent physical damage before fixation. Unfortunately, it is difficult to assess whether any changes to the red blood cells occur prior to fixation. In this context, the red blood cells from the AQP1 knockout mice serve as a control to rule out the presence of procedural artifacts. Additionally, it is possible, but unlikely, that blood loss or fixation causes a change of osmolarity within the medulla that only affects the wild-type cells. Red blood cell volume reduction of 40% is surprising when seen *in vivo* as this likely represents the total volume of free water found within the cell A typical erythrocyte contains approximately 35% v/v hemoglobin, 3-5% v/v salts and other proteins, with the remaining 60% being water. With the assumption that 30% of the total water is bound, approximately 40% of the total volume of the erythrocyte is free water. The results seen in the vasa recta of the kidney indicate that all, or nearly all, of the free water in red blood cells near the bottom of the medulla is transferred to the surrounding plasma. It may be possible to see further volume reduction under extreme hyperosmotic conditions, however this situation would be unlikely given normal physiology.

Contour and meshing for accurate volume measurement

The accuracy of contours made from confocal images relies only on the x/y resolution of the images. Transitioning from contours to 3D meshes requires high z-direction resolution of the image stack as well as good resolution of the contour itself. Resolution of the image stack in the z-direction, or the spacing between images in the stack, is important to the curvature of the cell between any two contours. Because meshing performs a linear approximation between points on two adjacent contours, having contours closer together reduces the error due to curvature. Thus, the importance of high z-direction resolution needs to be balanced with the need for large scale data collection which requires large spaces to be imaged.

Additionally, increasing resolution of the contour itself increases the number of triangular faces of the mesh which has the advantage of being able to more closely conform to complex shapes. Capping of meshes also creates an error as the first and last contour are assumed to be flat for consistency. Depending on the position of the red blood cell relative to the imaging surface, the final contours obtained may have large differences in surface area. In general, the larger the surface area of a capped contour, the more error will exist between the measured and the true volume. The morphology of the cells in the vasa recta of the kidney should also be considered. At 60% of the normal volume, most erythrocytes in the bottom of the medulla are expected to be crenated. Crenated erythrocytes appear spherical with small protruding spikes. 3D reconstructions of cells with reduced volumes appear mainly spherical and likely lack the necessary resolution to fully visualize any spikes. This effect would be biased towards the inner medulla and

might contribute to lower measured volumes than would otherwise be obtained with much higher *z*-resolution.

Histology and fixation of kidney sections

Kidney excision and immersion in fixative occurs in seconds after cervical dislocation however blood loss can occur and how this effects the red blood cells within the vasa recta is questionable. Without mechanical damage to the kidney, blood loss should only occur upon separation of the renal artery and vein. Thus, if blood loss were to affect the capillaries, an effect should first be visualized in the arterioles or larger veins. Measurements and observations from the kidney cortex and from the renal artery showed no defects in red blood cell morphology or deviations from expected cell size.

Another possible defect in morphology exists in the form of sharp angles occasionally observed in individual red blood cells within capillaries. During fixation, red blood cells packed together and can be separated by agitation post fixation. This causes flat surfaces to appear on these cells indicating regions that were in contact with other cells prior to fixation. The effect this would have on red blood cell volume is unknown however any change in volume due to such an effect would need to originate from an applied external pressure gradient. As the kidneys are unlikely to be vigorously agitated during incubation in fixative, this effect is likely to be a naturally existing condition or a result of the initial kidney excision and thus a short lived effect with minimal impact on final volume measurements. In addition, the morphology of observed red blood cells from the knockout mouse model suggested that the morphology of wild-type red blood cells were well preserved by the described methodology.

Negative imaging of red blood cells with confocal microscopy

The combination of DAB and ATTO 655 proved highly advantageous while imaging with a confocal microscope. The high contrast enabled easy identification of red blood cells at low magnifications and lowered the necessary resolution at high magnification to obtain accurate cell contours. Data collection with a confocal microscope can take longer than an hour per image stack depending on resolution which would typically make photobleaching of the target an issue. However with the fluorescent dye present outside of the target, most photobleaching effects are overcome by diffusion of excess dye from the mounting procedure. With a relatively high concentration of the dye, problems due to photobleaching effects are non-existent even with repeated imaging and long exposures. Additionally, the high contrast DAB and ATTO 655 provides allows for easy cell identification and image thresholding when attempting to create cell contours.

Implications of volume changes

It should also be noted that the large volume reductions observed here would have implications beyond water transport. A 40% volume reduction of a cell causes an increase in the concentration of all proteins and molecules. The rate of all chemical interactions would increase as a result of this. Whether this could affect oxygen delivery is unknown at this time. Additionally, reductions in cell size will change the viscosity of blood in a manner not too dissimilar to changing hematocrit. While hematocrit measures the number of cells with an assumed size, changes due to water transport would alter cell size while assuming a constant number of cells. While similar, these two effects would be related fundamentally through Einstein-Stokes relation. Thus the effect of a 40% volume reduction of all

erythrocytes should result in a decrease of the blood viscosity through these capillaries. Consideration should also be given to the structural aspects involved with large volume reductions. Erythrocyte interactions between themselves as well as with the walls of narrow capillaries would be altered by the reduction in volume as well as the associated change in morphology.

Chapter 1, in part is currently being prepared for submission for publication of the material. Sugie, Joseph; Sung, L. Amy. The dissertation author was the primary investigator and author of this material.

Supplementary Materials

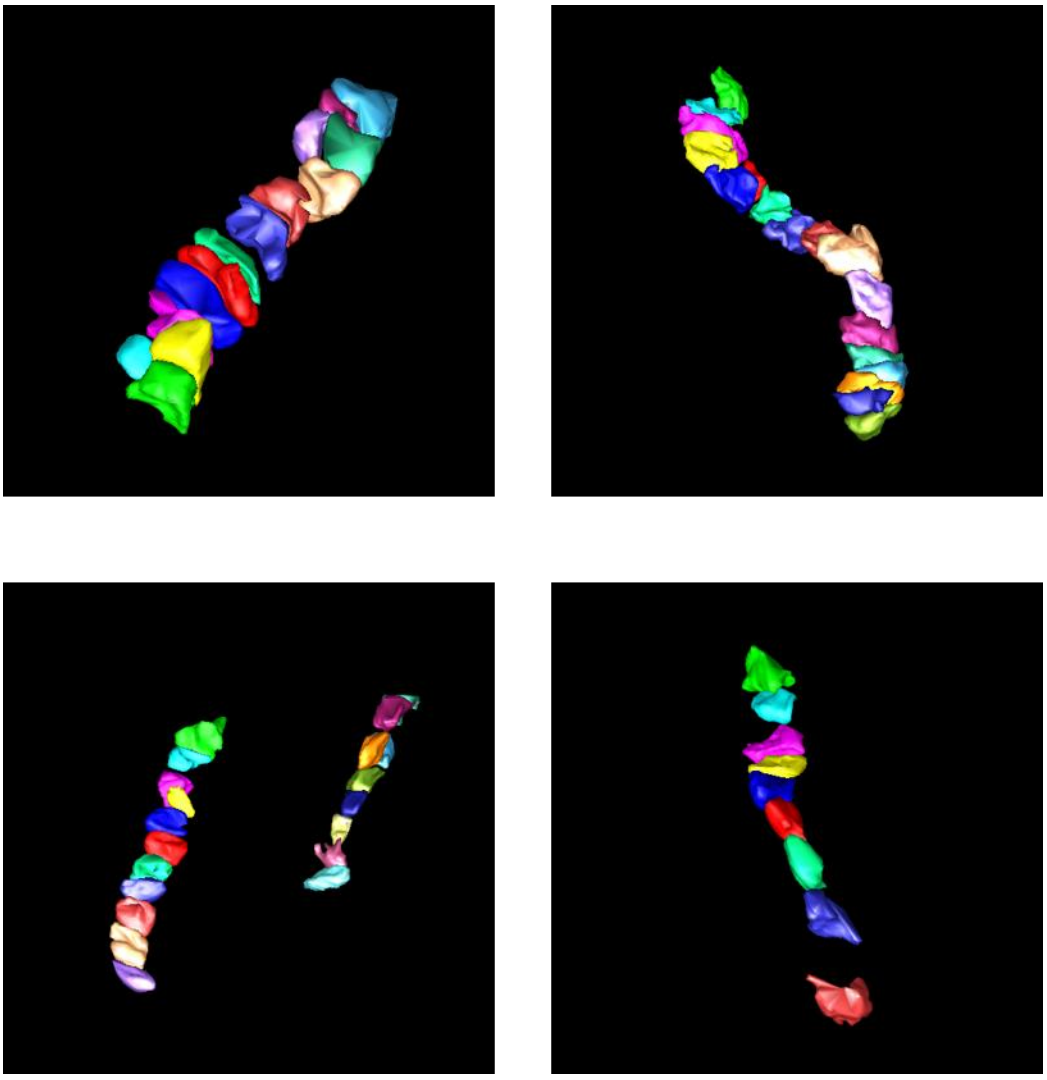

Figure S1.1 Fully meshed red blood cells located within vasa recta capillaries. Some red blood cells were packed and displaying sharp angles resulting from contact. Average length of capillary segments was limited by kidney section thickness (30 μm).

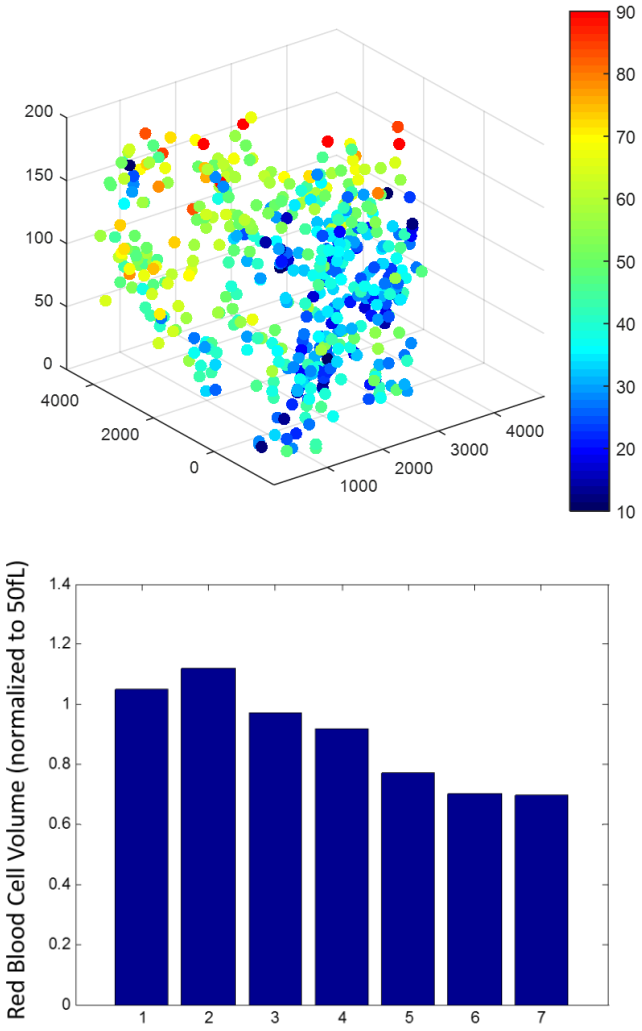

Figure S1.2 Red blood cell volume distribution from wild-type male mouse 1 kidney 1. Distribution is oriented with cortex on the left and medulla on the right. Color indicates cell volume in fL.

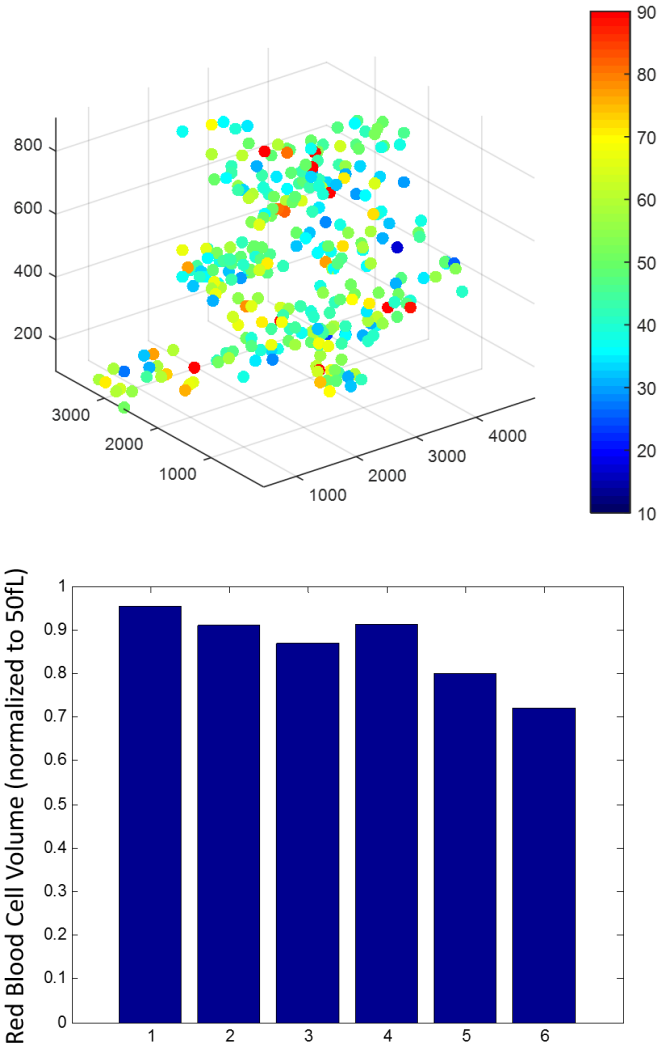

Figure S1.3 Red blood cell volume distribution from wild-type male mouse 1 kidney 2. Distribution is oriented with cortex on the left and medulla on the right. Color indicates cell volume in fL.

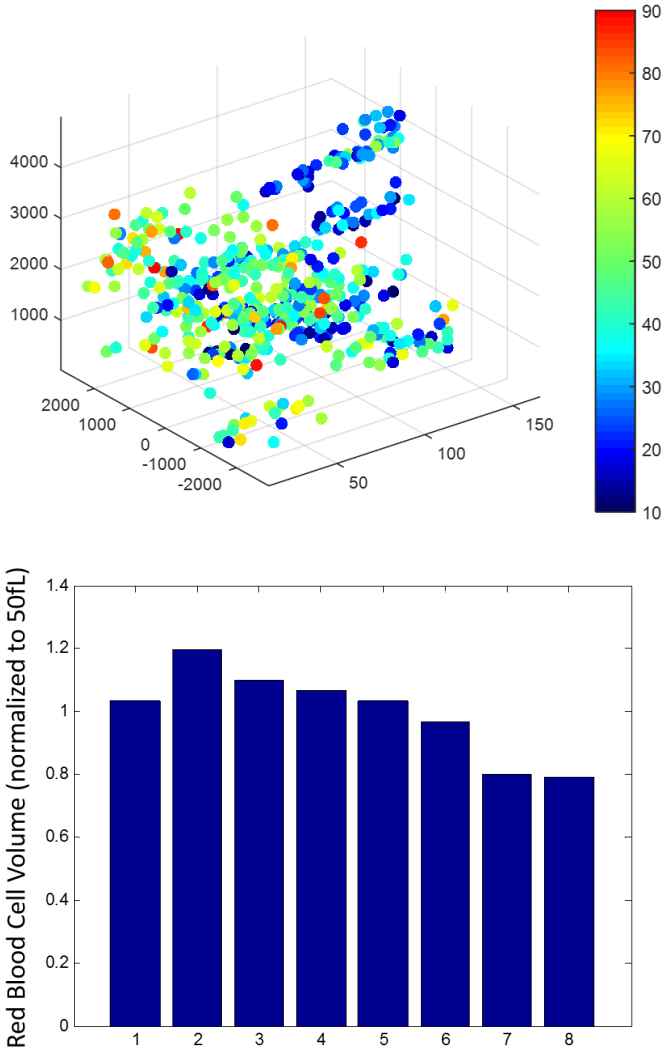

Figure S1.4 Red blood cell volume distribution from wild-type male mouse 2 kidney 1. Distribution is oriented with cortex on the left and medulla on the right. Color indicates cell volume in fL.

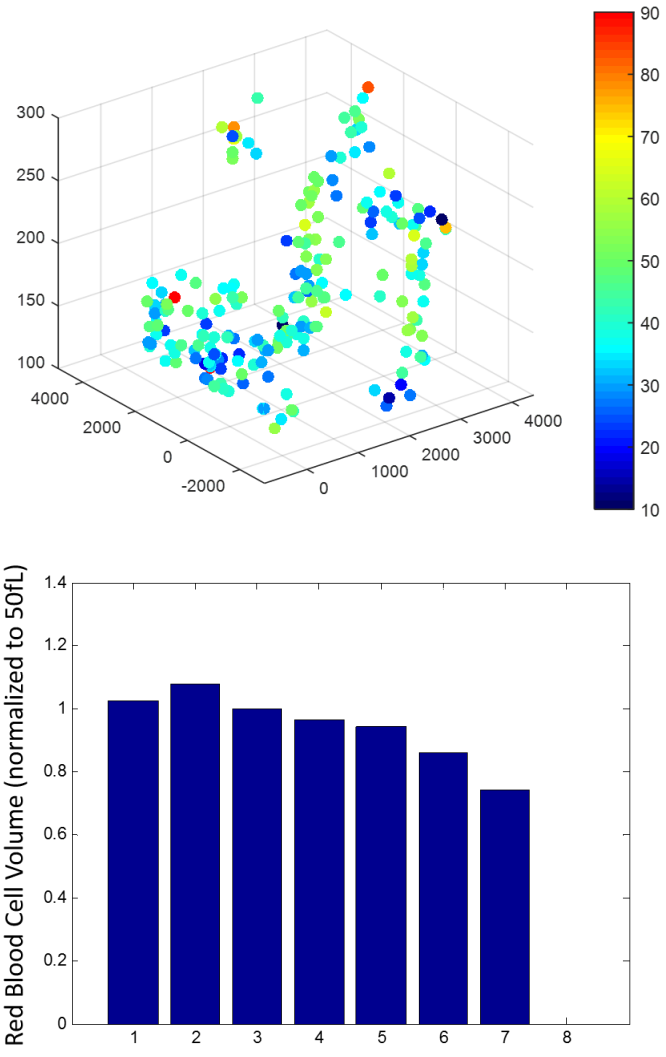

Figure S1.5 Red blood cell volume distribution from wild-type female mouse 1 kidney 1. Distribution is oriented with cortex on the left and medulla on the right. Color indicates cell volume in fL.

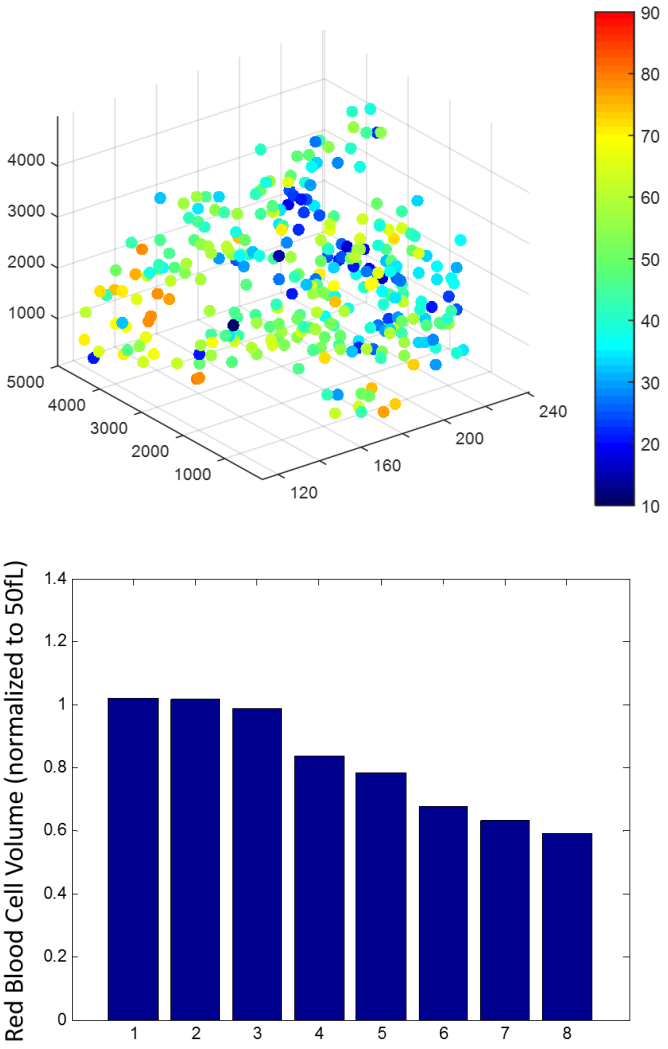

Figure S1.6 Red blood cell volume distribution from wild-type female mouse 2 kidney 1. Distribution is oriented with cortex on the left and medulla on the right. Color indicates cell volume in fL.

CHAPTER 2

Mathematical Modeling of Water Transport in the Capillary Systems Using Kedem-Katchalsky Membrane Equations

Introduction

Mathematical models for blood flow and membrane transport have been extensively studied for over a century. In order to expand and generalize beyond the specific systems studied in chapters 1 and 3, a simple mathematical model can be used to explore systems difficult to experiment on. Kedem-Katchalsky equations of membrane transport are simple and generalizable sets of equations to describe both fluid and solute flow across homogenous membranes [Salathe, E.P. and An, K., 1976; Kleinhans, F.W., 1998; Williams, M.E., 2003]. Critical to these equations is the assumption that fluid flow is driven by a linear combination of hydrostatic and osmotic pressure. Additionally, these equations require that membranes be largely homogenous to obtain bulk measurements of permeability. The capillary wall has been previously characterized within a 2-parameter formalism framework [Salathe, .E.P. and An, K., 1976]. The erythrocyte membrane contains 200,000 copies of AQP1 with no known bias in their distribution throughout [King et al., 2000]. Additionally, permeability of the erythrocyte membrane to water has been previously measured in both wild-type and AQP1 knockout mouse models [Yang et al., 2001].

Kedem-Katchalsky equations are a commonly used formalism to describe the fluid and solute flow between two well-mixed compartments separated by a membrane [Kleinhans, F.W., 1998]. While commonly applied to transport between the plasma and surrounding interstitial fluid, these equations are not typically used for transport across individual cell membranes. This is usually because the cytoplasm of a cell is not a good fit for the assumption of a well-mixed compartment. In the case of red blood cells, there is no nucleus or other cytoplasmic organelles except for a plasma membrane supported by a membrane skeletal network (no

significant metabolism) and the major components of water, hemoglobin, salts and small molecules. In addition, the membrane is highly deformable and the 3D organization of the spectrin-actin network may provide a mechanism for mixing the submembrane gradient [Sung and Vera, 2003]. Given the strain that red blood cells are consistently experiencing in the flow, especially in capillaries, as well as fact that more than 60% of the volume of the red blood cell is water, the well-mixed assumption is justifiable.

In addition to helping validate or predict aspects of experiments done in chapters 1 and 3, a model for water transport in a capillary that includes red blood cells can be useful to explore conditions that could not be easily observed *in vivo* or *in vitro*. Hematocrit in capillaries is often considered to be approximately 20% but this value can change from one capillary to another depending on bifurcation geometry and size [Fung, Y.C., 1973; Schmid-Schöenbein, G.W., Skalak, R. Usami, S. and Chien, S., 1980]. Individual red blood cell differences in microvasculature are difficult to examine experimentally and thus the use of a mathematical model aids in understanding trends within these systems.

Methods

A compartment-based system was established to create single units each consisting of 3 compartments: a red blood cell, surrounding plasma, and surrounding interstitial fluid. Figure 2.1 shows the general layout and relation between compartments in this system. Singular units can be arranged to form long capillaries and fluid flow simulated through the connection between units. By altering the initial solute concentrations in the interstitial fluid, external hypo or

hyperosmotic gradients are simulated. The general equations used to describe transport between each membrane-bound compartment are of the form:

$$J_v(x,t) = \rho_f V_w \left[\left(\left(C_i(x,t) - C_e(x,t)\right) + \sigma\left(C_{d,i}(x,t) - C_{d,e}(x,t)\right)\right) - \left(P_i(x,t) - P_e(x,t)\right)\right] \quad \text{eq. 1}$$

$$J_c(x,t) = (1-\sigma)\check{C}(x,t)J_v(x,t) + \rho_d\left(C_{d,e}(x,t) - C_{d,i}(x,t)\right) \quad \text{eq. 2}$$

These equations are general forms describing volume flow in equation 1 and associated solute flow in equation 2 between an internal and external compartment due to osmotic and hydrostatic pressures. In order to adapt them to the capillary and red blood cells parameters from table 2.1 are used.

The general equations (eq.1 and eq.2) were expanded to accommodate volume change of the red blood cell and have been rearranged to the more useful form seen in eq.3. In this form, concentration is separated into number of molecules and red blood cell volume to explicitly model the change in each. While eq. 3 is specific for the red blood cell, the same expansion is performed to generalize the equation to both the plasma and interstitial fluid compartments.

$$J_{v,RBC}(x,t) = \rho_f V_w \left[\frac{\left(\left(N_i(x,t) + \sigma N_{d,i}(x,t)\right) - \left(N_e(x,t) + \sigma N_{d,e}(x,t)\right)\right)}{V_{RBC}} - \left(P_i(x,t) - P_e(x,t)\right)\right] \quad \text{eq. 3}$$

The series of differential equations was solved using Matlab R2012a using a 0.1 ms timestep. Data was visualized as greyscale animation of osmolarity changes for each compartment as well as through graphs for variables of interest. Full code is provided in Supplementary Materials.

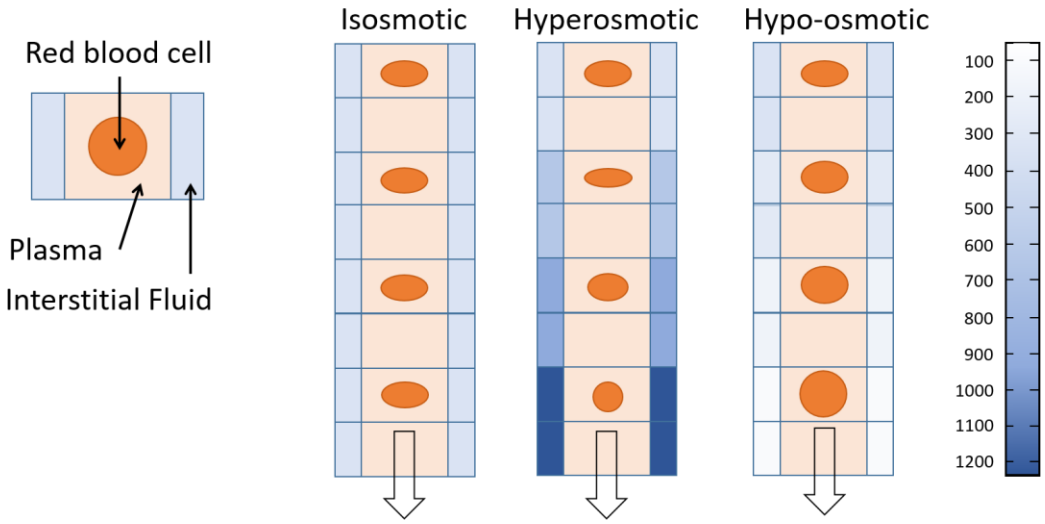

Figure 2.1 Schematic of single unit modeling approach. A single unit is made consisting of three compartments: a red blood cell, plasma and interstitial fluid. Hypo and hyperosmotic gradients are simulated by changing the initial osmolarity within the interstitial fluid.

Table 2.1 Major parameters for Kedem-Katchalsky applied to capillary water transport. General values used in simulation of capillary blood flow and water transport. Mean values from wild-type C57BL/6 mice used for red blood cell parameters. Permeability for WT and KO RBC adapted from the Verkman group [Yang et al. 2001]. Full references in supplementary.

RBC Volume	50 fL
RBC Diameter	6 um
Capillary Diameter	6 um
Capillary length	1 mm
Hematocrit	20%
Flow Speed	0.3 mm/s
RBC Permeability (p_f)	0.018 cm/s
KO Permeability (p_f)	0.003 cm/s
Molar Volume of Water (V_w)	18.03 cm^3/mol
Hydrodynamic conductivity	5E-11 cm^3/(s dyne) endo 4.5E-10 cm^3/(s dyne) gap
Interstitial Fluid Diameter	12 um
Reflection coefficient	0.95 – 0.99
Arterial Pressure P_{art}	32 mmHg
Venous Pressure P_{ven}	16 mmHg
Initial Blood Osmolarity	300 mOsM

Results

Simulation of Vasa Recta Capillaries

By setting a hyperosmotic concentration gradient in the interstitial fluid compartment of the model, a simulation approximating the vasa recta capillaries has been made. Because of the complexity of the countercurrent multiplier system described previously in chapter 1, the generation of the gradient was not explicitly simulated. Instead, the gradient was maintained at levels considered appropriate for a functioning kidney. In order to match previously described in *vivo* experimental conditions, red blood cell volume was observed to compare with results from Figure 1.6. Comparison using permeability from wild-type red blood cells and that from AQP1 knockouts are shown in Figure 2.2. Most notably, the change in red blood cell volume matches *in vivo* results showing a 38% decrease. Simulation of AQP1 knockout red blood cells displays a small decrease in red blood cell volume. This decrease is unlikely to match with *in vivo* results from the AQP1 knockout mouse models. These mice are known to have impaired kidney function and an inability to form a concentrated gradient in the medulla in contrast to the simulation which imposes a gradient matching wild-type measurements as no corresponding measurements for the knockout exist.

Comparison to results from chapter 1, particularly Figure 1.7 reveals a steady decrease in volume contrasting the volume increase seen from the cortex *in vivo*. Analysis of the current simulation reveals that a volume increase is impossible against a hyperosmotic gradient without either a sustained hypo osmotic section of the cortex or a large transient concentration flux that is not simulated under these conditions.

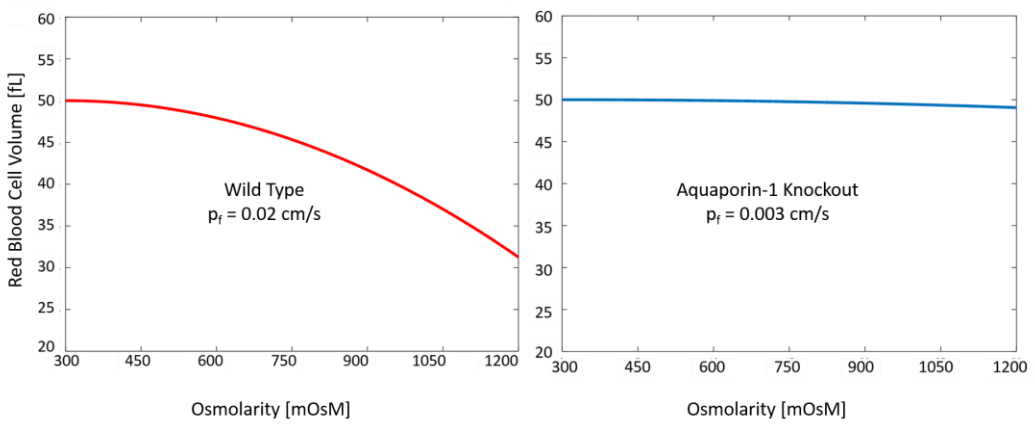

Figure 2.2 Simulation of wild-type and AQP1 knockout red blood cells in vasa recta capillaries. Wild-type red blood cells (left) show a 38% decrease compared to initial volume. Slight decrease in red blood cell volume is seen in AQP1 knockout (right). Model is simulated with a maintained hyperosmotic gradient in the interstitial fluid.

Hematocrit and blood flow speed changes against hypo and hyperosmotic interstitial gradients

Alterations of blood flow and hematocrit around mean values is necessary to understand how a capillary system will respond to fluctuations in speed or unusual bifurcations in microcirculation. Blood flow may be easily altered by changes to blood pressure whereas hematocrit can differ between capillaries depending on the geometry of the initial bifurcations [Fung, Y.C., 1973; Schmid-Schöenbein et al., 1980]. Changes to red blood cell volume are tracked during simulation to assess the impact on regulatory capabilities.

Trends in blood flow alteration show expected results. Slower blood flow enables longer times for water exchange between the capillary and the interstitial fluid. Faster blood flow enables quicker washout of hypo or hyperosmolarity which places less stress on red blood cells. Slower blood flow relies more on the regulatory capabilities of red blood cells. Figure 2.3 demonstrates the trends in changing blood flow velocity. Particularly, slow blood flow through hypo or hyperosmotic gradients causes a larger reliance on red blood cells to reduce osmotic pressure in the plasma. With a large enough gradient and blood flow reduced to one quarter the normal speed, crenation and possibly lysis of red blood cells could occur. Interestingly, it appears that increasing blood flow provides no negative effects on red blood cell volume or plasma water balance. In fact, as blood flow speed increases, the need for red blood cells to act as regulators decreases.

Similarly, changing hematocrit creates a comparable trend. Increasing the number of red blood cells reduces the amount of water needed from any individual blood cell. Figure 2.4 shows that low capillary hematocrit increases the overall osmotic pressure each individual red blood cell experiences. As a result, red blood

cell volume change is the greatest for low hematocrit. Similar to blood flow velocity, a low hematocrit in conjunction with large hypo or hyperosmotic gradients can cause red blood cells to lyse or crenate respectively. However, intravascular hemolysis is normally not observed, suggesting there are other potential constrains or mechanisms preventing this from happening. Reduction in hyperosmotic condition in the renal system (up to 1200 mOsM) did not go beyond 38% or the limit.

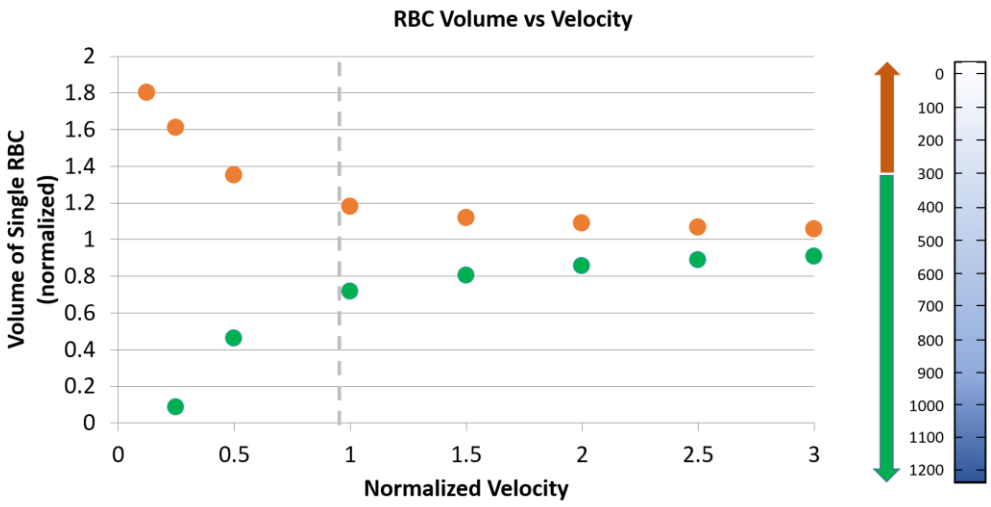

Figure 2.3 Volume of wild-type red blood cells simulated against hypo and hyperosmotic interstitial gradients with different blood flow velocities. Both hypo (orange) and hyper (green) represent a similar trend of greater reliance on red blood cells for slower blood flow velocity. A combination of low blood flow speed against hypo or hyperosmotic gradients can potentially cause lysis or crenation *in vivo*.

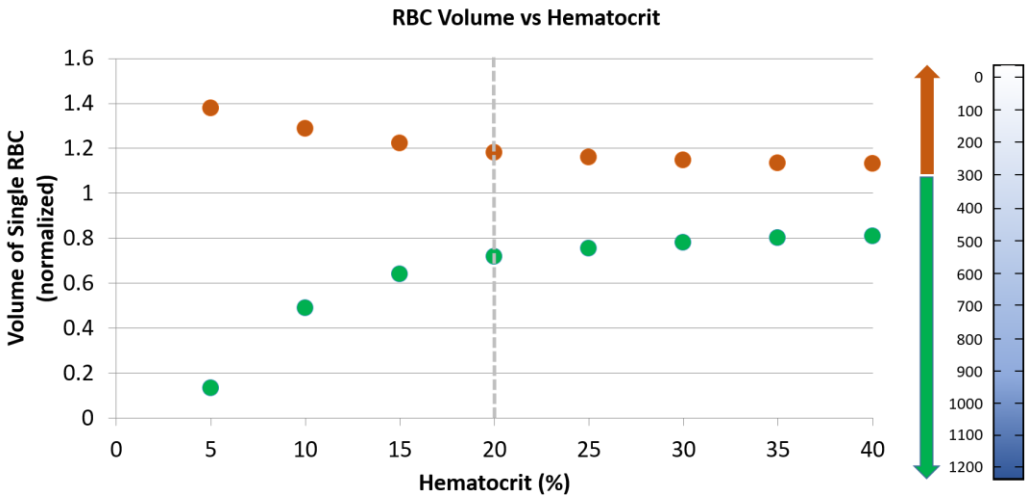

Figure 2.4 Volume of wild-type red blood cells simulated against hypo and hyperosmotic gradients under different hematocrit. Both hypo (orange) and hyperosmotic (green) show similar trends of increasing reliance on red blood cells for decreasing hematocrit. Less red blood cells creates a greater stress on each individual red blood cell.

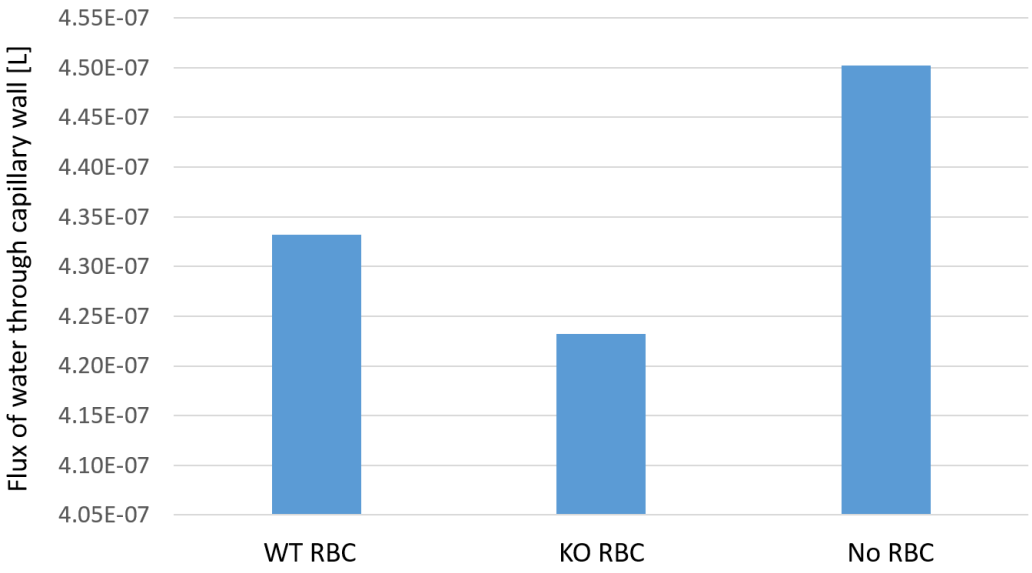

Figure 2.5 Transfer of water through the vasa recta capillary wall for three simulated conditions. Total water flux through the capillary wall calculated over 30 seconds. In the condition without red blood cells there is more plasma which has higher water content than red blood cells. The low permeability of AQP1 knockout red blood cells effectively reduces the amount of water capable of being transported.

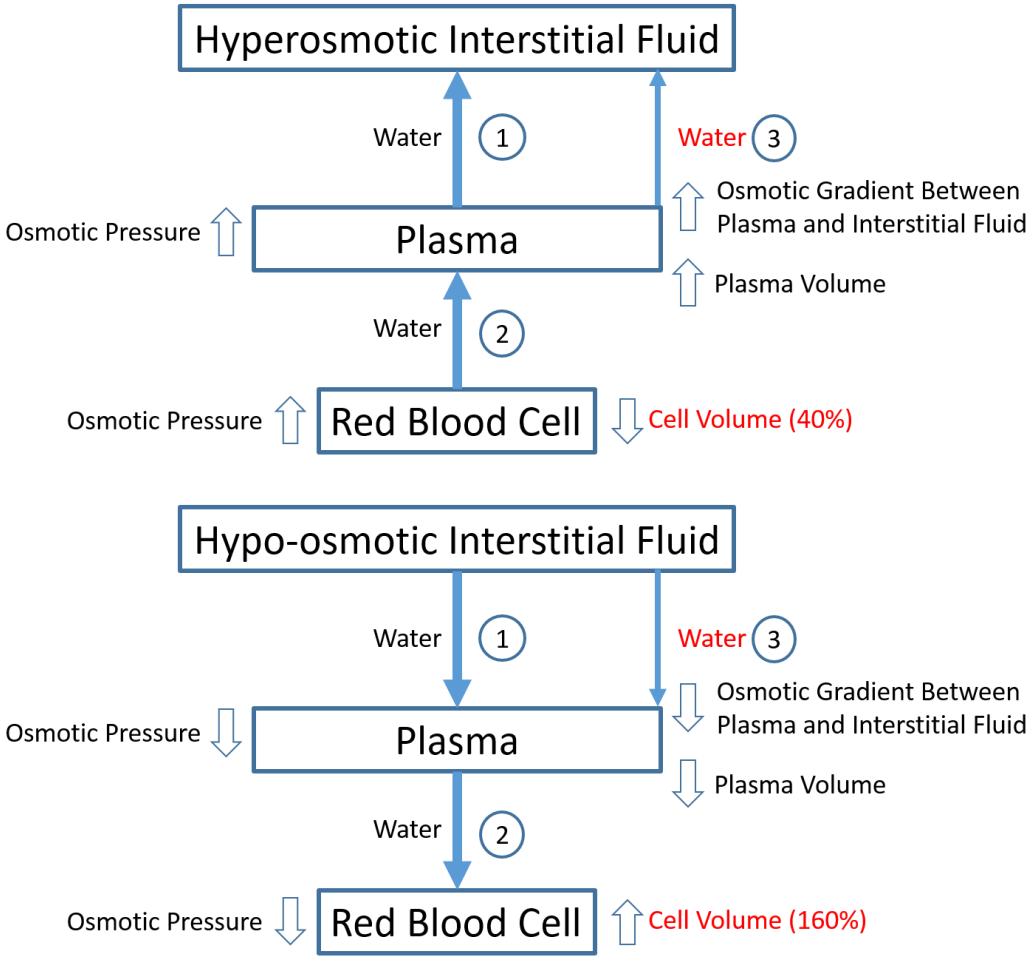

Figure 2.6 Red blood cells as micropumps. Combining results from all simulations leads to the hypothesis that red blood cells act as miniature pumps in microcirculation. Against an external hypo or hyperosmotic gradient, red blood cells act rehydrate or dehydrate surrounding tissue by increasing the speed at which water that passes through the capillary wall.

In Figure 2.5, the total useable water content is the major predictor for the ability to rehydrate surrounding tissues. Plasma has higher water content than red blood cells due to the large volume occupied by hemoglobin. Thus the presence of red blood cells lowers the total amount of water within the capillary. With low water permeability, this reduction of water is the total red blood cell volume. Higher permeability would make the otherwise trapped water, accessible. The high water permeability that AQP1 allows makes the free water of the red blood cell capable of water balance regulation. Additionally, this suggests that the presence of red blood cells helps to maintain the gradient within the kidney by reducing the washout that would otherwise occur.

Red blood cells as micropumps

Combining results from all simulations lead to the development of the idea that red blood cells act as miniature pumps in microcirculation. Figure 2.6 illustrates that in the hypo-osmotic condition, initial water transport into erythrocytes increases the cell volume, decreases the plasma space, increases the concentration of the plasma, and the gradient across the capillary wall, thus further facilitating the transport of water from the interstitial space. Similarly in the hyperosmotic condition, transport of water out into the plasma, decreases cell volume. Reducing cell volume effectively increases the volume of plasma, thus reducing the concentration of molecules in plasma and increasing the gradient across the capillary wall, which facilitates water transfer into the interstitial space. This outlines the fundamental idea that red blood cells increase the amount of water passing through the capillary wall because of their rapid water transport capabilities and their ability to change volume in response to internal water loss

and gain. However, the total water loss and gain is limited by the capacity of cell volume changes. The red blood cells are able to reduce their volume up to 40% and increase by 160%, at that level, red blood cell would lyse.

Discussion

Water transport across the capillary wall

Evaluating the regulatory capability of red blood cells includes their effectiveness in maintaining water homeostasis. Simulations revealed that red blood cells with AQP1 enable more water to pass through the capillary wall compared to AQP1 knockout cells. Although a capillary without red blood cells rehydrated surrounding tissue the most and may appear to be the most efficient, this result should be interpreted carefully.

First, the capillary without red blood cells was simulated with the blood consisting entirely of plasma. This means that there was no volume occupied by hemoglobin. Arguably, because the difference in water content between plasma and red blood cells is primarily due to hemoglobin, the difference between these two simulated conditions is unlikely to be caused by membrane water permeability alone. With an equivalent volume of hemoglobin simulated in the plasma and a perfectly permeable membrane, the results would be expected to be nearly identical. Additionally, lack of hemoglobin in the blood is a system that is not physiologically relevant for mammals. In this context, the red blood cell can be seen as a good compromise between oxygen delivering and water transport capabilities.

Variations of blood flow and hematocrit

Simulations varying blood flow velocity and hematocrit demonstrated the importance of red blood cells. Both series of simulations displayed an increased reliance on red blood cells as blood flow velocity or hematocrit dropped below normal values. Thus, plasma alone would likely be inadequate by comparison. While variations in hematocrit can occur regularly, sudden drops in blood flow are typically associated with pathological conditions. Therefore, functioning red blood cells are predicted to play a role in preventing the development of exacerbated conditions stemming from low blood pressure.

It is interesting to note that the trend seen in varying blood flow and hematocrit are similar when considered from the frame of reference of the tissue. The effect of slowing blood flow or reducing the number of blood cells present both result in less red blood cells moving by the tissue in a given timeframe. As hypo or hyperosmotic gradient in the tissue is the driving force for water transport, it is unsurprising that trends seen here are similar to each other.

Simulation of vasa recta capillaries

Simulations representing capillaries in the kidney medulla were primarily characterized by the static, hyperosmotic gradient in the interstitial fluid. Allowing this concentration gradient to decrease from the water transport of plasma and red blood cells would need to be balanced by generation of the gradient from the loop of Henle. Previous simulations have demonstrated the complexity required to fully simulate the countercurrent mechanism responsible for a hyperosmotic interstitial fluid [Pallone et al., 2000; Layton, A.T., 2007; Layton, A.T. and Layton, H.E., 2011]. In addition, studies since the original proposal of the countercurrent multiplier

system suggest that details of the urine concentrating mechanism are still unknown [Kokko, J.P. and Rector, F.C., 1972; Layton et al., 2004]. Because of these difficulties, the model was simplified to reflect measurements of interstitial osmolarity which have remained as reputable values since their original publication in 1959 [Gottschalk, C.W. and Mylle, M., 1959]. Thus, the assumption is made that these original measurements were obtained from a steady-state within the kidney medulla which justifies their unchanging nature within these simulations. Any change to interstitial concentration resulting from plasma or red blood cell water transport is simultaneously and equally balanced by generation from the loop of Henle.

Chapter 2, in part is currently being prepared for submission for publication of the material. Sugie, Joseph; Sung, L. Amy. The dissertation author was the primary investigator and author of this material.

Supplementary Materials

Matlab 2015a code for general modeling of capillary systems

```
close all;
clear all;
clc;
%test flow
%fluxes
%RBC=1
%plasma=2
%endo=3
%isf=4
%data from multiple pathways of...

t_step=0.0001;
t_end=30;
t_tot=t_end/t_step;
t=t_step:t_step:t_end;

%assuming 1mm long capillary with 20% hemocrit => 5um long boxes => 200
%boxes
vx_rbc=(1E-3/4)*0.001; %m/s  (1 mm/s)
vx_pla=(1E-3*0.75/4)*0.001; %m/s
vnx_pla=(1E-3*0.75/4); %m/s
%vnx_pla=1E-3; %m/s
cap_length=1E-3; %m
hemo=0.20;
%pf_rbc=0;
pf_rbc=0.02;
%pf_rbc=0.0013;%cm/s
Lp_endo=5E-11;  %cm^3/sdyne
Lp_inter=4.5E-10; %cm^3/sdyne
r=3;
V0_rbc=0.50E-10;  %cm^3
no_sections=hemo*100^3*1E-3*3.14*(r*10^-6)^2/V0_rbc;
no_sections=round(no_sections);
V0_pla=3.14*(r*10^-6)^2*(1/no_sections)*cap_length*100*100*100-
V0_rbc;  %cm^3 4um radius
%V0_endo=3.958E-10; %cm^3
r_isf=6;
V0_isf=3.14*(r_isf*10^-6)^2*(1/no_sections)*cap_length*100*100*100-
V0_pla; %cm^3 6um radius
A_rbc=0.9E-6;  %cm^2
A_pla=3.14*2*(r*10^-6)*(1/no_sections)*cap_length*100*100*0.99;   %cm^2 total
99%
```

```
A_gap=3.14*2*(r*10^-6)*(1/no_sections)*cap_length*100*100*0.01; %cm^2 total
1%
%A_endo=8.134E-6;  %cm^2
PMVW=18; %cm^3/mol
M_rbc = zeros(no_sections,t_tot);
M_pla = zeros(no_sections,t_tot);
Mc_rbc = zeros(no_sections,t_tot);
Mc_pla = zeros(no_sections,t_tot);
M_isf = zeros(no_sections,t_tot);
Mc_isf = zeros(no_sections,t_tot);

%for i=1:1:no_sections
%                                                          M_isf(i,1)          =
V0_isf*(300/1000)/1000+V0_isf*(900/1000)/1000*(i/no_sections); %Osm
%end
P_pla=zeros(no_sections);
for i=1:1:no_sections
    P_pla(i)=32-(i-1)/no_sections*16; %mmHg
    %P_pla(i)=0;
end
%P_isf=38; %mmHg
P_isf=16;
T=310.15; %K
RT=19332.53; %L*mmHg/mol
dyneconversion=(1E6)/750.06; %(10^6dyne/cm^2)/750.06mmHg
refcoef_rbc=0.9;
refcoef_pla=0.9;
refcoef_gap=0.1;

V_rbc=zeros(no_sections,t_end/t_step);
V_pla=zeros(no_sections,t_end/t_step);
V_isf=zeros(no_sections,t_end/t_step);

%NO RBCs
Vn0_pla=3.14*(r*10^-6)^2*(1/no_sections)*cap_length*100*100*100-
V0_rbc; %no rbc transport
%Vn0_pla=3.14*(r*10^-6)^2*(1/no_sections)*cap_length*100*100*100; %no rbc
Vn0_isf=3.14*(r_isf*10^-6)^2*(1/no_sections)*cap_length*100*100*100-
V0_pla; %cm^3 6um radius
Vn_pla=zeros(no_sections,t_end/t_step);
Vn_isf=zeros(no_sections,t_end/t_step);
Mn_pla=zeros(no_sections,t_tot);
Mn_isf=zeros(no_sections,t_tot);
Mnc_pla=zeros(no_sections,t_tot);
Mnc_isf=zeros(no_sections,t_tot);

Tavg_temp=0;
k=0;
l=0;
```

```
V_rbc_temp=zeros(1,no_sections);
M_rbc_temp=zeros(1,no_sections);
Mc_rbc_temp=zeros(1,no_sections);
V_pla_temp=zeros(1,no_sections);
M_pla_temp=zeros(1,no_sections);
Mc_pla_temp=zeros(1,no_sections);
for i=1:1:(t_end/t_step)
   k=k+1;
   l=l+1;
   Tstart=tic;
   for j=1:1:no_sections
   if i == 1
      V_rbc(j,1)=V0_rbc;
      V_pla(j,1)=V0_pla;
      V_isf(j,1)=V0_isf;
      M_rbc(j,1) = V0_rbc*(300/1000)/1000; %Osm
      M_pla(j,1) = V0_pla*(300/1000)/1000; %Osm
      M_isf(j,1)                                                                    =
V0_isf*(300/1000)/1000+V0_isf*(900/1000)/1000*(j/no_sections); %Osm
      Mc_rbc(j,1) = V0_rbc*(1.66/1000)/1000;
      Mc_pla(j,1) = V0_pla*(1.66/1000)/1000;
      Mc_isf(j,1) = V0_isf*(0.776/1000)/1000;
   else
      J_rbc_pla=-pf_rbc*A_rbc*PMVW*refcoef_rbc*((M_rbc(j,i-1)+Mc_rbc(j,i-
1))/V_rbc(i-1) - (M_pla(j,i-1)+Mc_pla(j,i-1))/V_pla(i-1));
      J_pla_isf=Lp_endo*A_pla*dyneconversion*((P_pla(j)-P_isf)-
refcoef_pla*RT*((M_pla(j,i-1)+Mc_pla(j,i-1))/V_pla(j,i-1)-(Mc_isf(j,i-1)+M_isf(j,i-
1))/V_isf(j,i-1)));
      J_pla_gap=Lp_inter*A_pla*dyneconversion*((P_pla(j)-P_isf)-
refcoef_gap*RT*((M_pla(j,i-1)+Mc_pla(j,i-1))/V_pla(j,i-1)-(Mc_isf(j,i-1)+M_isf(j,i-
1))/V_isf(j,i-1)));
      V_rbc(j,i)=V_rbc(j,i-1)-J_rbc_pla*t_step;
      V_pla(j,i)=V_pla(j,i-1)+(J_rbc_pla-J_pla_isf-J_pla_gap)*t_step;
      V_isf(j,i)=V_isf(j,i-1)+(J_pla_isf+J_pla_gap)*t_step;
      C_prime_rbc=(M_rbc(j,i-1)-M_pla(j,i-1))/log(M_rbc(j,i-1)./M_pla(j,i-1));
      Js_rbc_pla=(1-refcoef_rbc)*C_prime_rbc*J_rbc_pla;
      C_prime_pla=(M_pla(j,i-1)-M_isf(j,i-1))/log(M_pla(j,i-1)./M_isf(j,i-1));
      Js_pla_isf=(1-refcoef_pla)*C_prime_pla*(J_pla_isf+J_pla_gap);
      M_rbc(j,i) = M_rbc(j,i-1)-Js_rbc_pla*t_step;
      M_pla(j,i) = M_pla(j,i-1)+(Js_rbc_pla-Js_pla_isf)*t_step;
      M_isf(j,i) = M_isf(j,i-1)+Js_pla_isf*t_step;
      Mc_rbc(j,i) = Mc_rbc(j,i-1);
      Mc_pla(j,i) = Mc_pla(j,i-1);
      Mc_isf(j,i) = Mc_isf(j,i-1);

      %rbc flow vx=(cap_length/no_sections)/t_step
      t_flow_rbc=cap_length/(no_sections*vx_rbc)/t_step;
      t_flow_rbc=round(t_flow_rbc);
```

```
if k==t_flow_rbc
    if j==1
        V_rbc_temp(j) = V_rbc(j,i);
        M_rbc_temp(j) = M_rbc(j,i);
        Mc_rbc_temp(j) = Mc_rbc(j,i);
        V_rbc(j,i) = V0_rbc;
        M_rbc(j,i) = V0_rbc*(300/1000)/1000;
        Mc_rbc(j,i) = V0_rbc*(1.66/1000)/1000;
    elseif j==no_sections
        k=0;
        V_rbc(j,i) = V_rbc_temp(j-1);
        M_rbc(j,i) = M_rbc_temp(j-1);
        Mc_rbc(j,i) = Mc_rbc_temp(j-1);
    else
        V_rbc_temp(j) = V_rbc(j,i);
        M_rbc_temp(j) = M_rbc(j,i);
        Mc_rbc_temp(j) = Mc_rbc(j,i);
        V_rbc(j,i) = V_rbc_temp(j-1);
        M_rbc(j,i) = M_rbc_temp(j-1);
        Mc_rbc(j,i) = Mc_rbc_temp(j-1);
    end
else
    k=k;
end

%pla flow vx=(cap_length/no_sections)/t_step
t_flow_pla=cap_length/(no_sections*vx_pla)/t_step;
t_flow_pla=round(t_flow_pla);
if l==t_flow_pla
    if j==1
        V_pla_temp(j) = V_pla(j,i);
        M_pla_temp(j) = M_pla(j,i);
        Mc_pla_temp(j) = Mc_pla(j,i);
        V_pla(j,i) = V0_pla;
        M_pla(j,i) = V0_pla*(300/1000)/1000;
        Mc_pla(j,i) = V0_pla*(1.66/1000)/1000;
    elseif j==no_sections
        l=0;
        V_pla(j,i) = V_pla_temp(j-1);
        M_pla(j,i) = M_pla_temp(j-1);
        Mc_pla(j,i) = Mc_pla_temp(j-1);
    else
        V_pla_temp(j) = V_pla(j,i);
        M_pla_temp(j) = M_pla(j,i);
        Mc_pla_temp(j) = Mc_pla(j,i);
        V_pla(j,i) = V_pla_temp(j-1);
        M_pla(j,i) = M_pla_temp(j-1);
        Mc_pla(j,i) = Mc_pla_temp(j-1);
    end
```

```
        else
            l=l;
        end


    end
    end

    T_temp=toc(Tstart);
    Tavg_temp=(Tavg_temp+T_temp);
    Tavg=Tavg_temp/i;
    estime=((t_tot-i)*Tavg)/60;
    estimated_time_temp=uint8([fix(estime) mod((t_tot-i)*Tavg,60)]);
    if mod(i,1000) == 0
        clc;
        remaining=t_tot-i
        if mod((t_tot-i)*Tavg,60) < 10
            RBC_estimated_time=[num2str(estimated_time_temp(1))          ':'          '0'
num2str(estimated_time_temp(2))]
        else
            RBC_estimated_time=[num2str(estimated_time_temp(1))                    ':'
num2str(estimated_time_temp(2))]
        end
    else
        RBC_estimated_time=[num2str(estimated_time_temp(1))          ':'          '0'
num2str(estimated_time_temp(2))];
    end
end



dlmwrite('h20isfosm300_1200P32_6KO\V_rbc.txt',V_rbc,'delimiter','\t');
dlmwrite('h20isfosm300_1200P32_6KO\V_pla.txt',V_pla,'delimiter','\t');
dlmwrite('h20isfosm300_1200P32_6KO\V_isf.txt',V_isf,'delimiter','\t');
dlmwrite('h20isfosm300_1200P32_6KO\M_rbc.txt',M_rbc,'delimiter','\t');
dlmwrite('h20isfosm300_1200P32_6KO\M_pla.txt',M_pla,'delimiter','\t');
dlmwrite('h20isfosm300_1200P32_6KO\M_isf.txt',M_isf,'delimiter','\t');
dlmwrite('h20isfosm300_1200P32_6KO\Mc_rbc.txt',Mc_rbc,'delimiter','\t');
dlmwrite('h20isfosm300_1200P32_6KO\Mc_pla.txt',Mc_pla,'delimiter','\t');
dlmwrite('h20isfosm300_1200P32_6KO\Mc_isf.txt',Mc_isf,'delimiter','\t');
Osm_pla=zeros(no_sections,t_tot);
NORBC_Osm_pla=zeros(no_sections,t_tot);
for i=1:1:no_sections
    for j=1:1:t_tot
        Osm_pla(i,j)=(M_pla(i,j)+Mc_pla(i,j))./V_pla(i,j)*1E6;
        NORBC_Osm_pla(i,j)=(Mn_pla(i,j)+Mnc_pla(i,j))./Vn_pla(i,j)*1E6;
    end
end
```

```
vidObj = VideoWriter('h20isfosm300_1200P32_6KO\capillary_press_pla.avi');
open(vidObj);

% Create an animation.
plot([1],[1])
getframe(gcf);
for i=1:1000:t_end/t_step
    i
    figure(1)
    subplot(1,2,1); imagesc(Osm_pla(:,i),[50 1250]);
    title('PLASMA')
    colorbar
    colormap(flipud(gray))
   % Write each frame to the file.
   currFrame = getframe(gcf);
   writeVideo(vidObj,currFrame);
end

% Close the file.
close(vidObj);

Osm_isf=zeros(no_sections,t_tot);
NORBC_Osm_isf=zeros(no_sections,t_tot);
for i=1:1:no_sections
    for j=1:1:t_tot
        Osm_isf(i,j)=(M_isf(i,j)+Mc_isf(i,j))./V_isf(i,j)*1E6;
        NORBC_Osm_isf(i,j)=(Mn_isf(i,j)+Mnc_isf(i,j))./Vn_isf(i,j)*1E6;
    end
end

vidObj = VideoWriter('h20isfosm300_1200P32_6KO\capillary_press_isf.avi');
open(vidObj);

% Create an animation.
plot([1],[1])
getframe(gcf);
for i=1:1000:t_end/t_step
    i
    figure(2)
    subplot(1,2,1); imagesc(Osm_isf(:,i),[50 1250]);
    title('ISF')
    colorbar
    colormap(flipud(gray))
   % Write each frame to the file.
   currFrame = getframe(gcf);
   writeVideo(vidObj,currFrame);
end

% Close the file.
```

```
close(vidObj);

figure(5)
plot(t,V_rbc(no_sections,:))
axis([0 30 2E-11 6E-11])

saveas(gcf,'h20isfosm300_1200P32_16KO\rbcvolume.jpg')

%figure(6)
%plot(Osm_isf(:,1))

%figure(7)
%plot(P_pla)

V_rbc(no_sections,t_tot)
```

Table S2.1 Major parameters for Kedem-Katchalsky applied to capillary water transport extended. Extended table of values to included citations.

RBC Volume	50 fL	Charles River Labs C57BL/6 Mouse Hematology Data sheet
RBC Diameter	6 um	Charles River Labs C57BL/6 Mouse Hematology Data sheet
Capillary Diameter	6 um	[Marieb, E.N. and Hoehn, K., 2013]
Capillary length	1 mm	Assumed value based on [Layton, A.T. and Layton, H.E., 2005]
Hematocrit	20%	[Fung, Y.C., 1973]
Flow Speed	0.3 mm/s	
RBC Permeability (p_f)	0.018 cm/s	[Yang et al., 2001]
KO Permeability (p_f)	0.003 cm/s	[Yang et al., 2001]
Molar Volume of Water (V_w)	18.03 cm^3/mol	Common value
Hydrodynamic conductivity	5E-11 cm^3/(s dyne) endo 4.5E-10 cm^3/(s dyne) gap	[Renkin, E.M., 1977]
Interstitial Fluid Diameter	12 um	Assumed value
Reflection coefficient	0.95 – 0.99	[Renkin, E.M., 1977; Kleinhans, F.W.]
Arterial Pressure P_{art}	32 mmHg	[Marieb, E.N. and Hoehn, K., 2013]
Venous Pressure P_{ven}	16 mmHg	[Marieb, E.N. and Hoehn, K., 2013]
Initial Blood Osmolarity	300 mOsM	[Marieb, E.N. and Hoehn, K., 2013]

CHAPTER 3

Examining the Regulatory Effect of Red Blood Cells on Osmolarity in a Microfluidic Device

Introduction

Measurements in the kidney demonstrate the ability of the red blood cell to respond to surroundings *in vivo*. Critical to understanding the regulatory role of red blood cells is evaluating the effect they can have on their surroundings. Measuring a significant effect on osmolarity from red blood cells within the plasma or tissue *in vivo* is difficult as the system has already reached a pseudo-steady state and the portion of any change due to red blood cells would need to be differentiated from any other coupled or simultaneous changes. Thus, a microfluidic chip designed to simulate flow in microcirculation creates an ideal environment to study as every aspect can be manipulated and each effect isolated. By using a carefully designed channel made to replicate capillary flow conditions, observations can be made about the kinetics of the red blood cell volume change. Additionally, direct measurements of the change in the surrounding fluid should be made and can be accomplished with a fluorescent marker of known concentration. Combined, this information will facilitate the understanding of the regulatory capabilities of red blood cells.

A microfluidic chip is a general term for a wide variety of devices that allow for microliter volumes of fluid to flow through a series of channels. Chip materials are commonly a form of plastic or glass composites and can be manufactured to be reusable or disposable, depending on the application. For a chip replicating a capillary, the simplicity of the design combined with the technical challenges of a viscous cell suspension make disposable chips advantageous. Because capillaries typically have 20% hematocrit, cell clumping which may cause channel blockages could easily render the device unusable. Additionally, viscous cell suspensions flowing through small channels requires high hydrostatic pressures

to achieve flow. Points of stress on the chip such as the surface between the polydimethylsiloxane (PDMS) and glass coverslip and the inlet or outlet ports could fail because of this. Therefore, multiple, disposable microfluidic devices are preferable to a single, precisely manufactured chip.

One of the major disadvantages of disposable chips is that any variation in the manufacturing of the mold will result in variations between each chip. In complicated chip designs, the chance for small defects in a mold becomes much higher. Because a chip replicating capillary flow can be designed with only a single layer, large defects are unlikely without physical damage to the silicon mold. In addition, inlet and outlet ports on disposable chips are made by hand. Typically, variation in port construction will only affect the difficulty of the experimental set up. Unfortunately, because of the high hydrostatic pressures involved with capillary-like flow, a poorly made port can rupture causing total device failure..

Microfluidic chips for the analysis of blood are not novel. However, studies which aim to fully replicate capillary blood flow have rarely been attempted. Most studies involving blood in microfluidics attempted to solve cell sorting problems which require drastically different design and flow conditions [Toner, M. and Irimia, D., 2005]. Several studies that observe the mechanics of blood flow have been done using a PDMS chip to analyze erythrocyte membrane mechanics [Tomaiuolo et al., 2011]. However, most similar studies examine forces on single cells using red blood cell suspensions of less than 1% hematocrit. Significant cell adhesion and clumping problems only become apparent for microfluidics when approaching 20% hematocrit.

The main goal of the *in vitro* design here is to isolate the effect that erythrocytes have on their immediate surrounding environment. While observed

red blood cell volume changes are assumed to cause corresponding changes to plasma, direct measurements from the extracellular fluid would confirm this. Thus, a fluorescent reporter was deemed desirable to obtain real time quantifiable data on a sufficient timescale. Several fluorescent molecules were considered with SYTOX green, a common viability stain, being chosen for two main advantages of use in in this system. First, as a viability stain, the dye is membrane impermeable and will remain only in the extracellular or plasma space. Keeping the dye out of red blood cells and exclusively in the surrounding fluid means that changes to the fluorescence correspond exactly to changes in the surrounding fluid once light scattering effects are removed. Second, the intended use as a viability stain ensures that the dye does not cause perceptible harm to living cells and its presence will not affect the system in a significant way.

Methods

Methods of microfluidic chip design and the full protocol for photolithography of the silicon wafer mold are detailed by the Hasty group in chapter 14 of Synthetic Biology: Methods for part/device characterization and chassis engineering [Voigt, C., 2011].

Microchip channel design

The chip was designed to include a long 10 μm x 10 μm x 2,000 μm channel to act as a capillary as well as a mixing W-junction to allow alterations of mixing osmolarity without physically disconnecting or swapping anything from the chip itself. The W-junction functions by taking a high osmolarity solution and a low osmolarity solution and mixing them in proportion to the hydrostatic pressure of

each. The two inputs to the W-junction flow into 3 outputs. Two outputs are waste channels designed to take the excess flow from both inputs. The remaining center channel allows the two inputs to mix. Any hydrostatic pressure difference between the two inputs manifests as a difference in the ratio between the two in the center channel. Calibration of this mixing is done by identifying the minimum pressures needed to create 100% low osmolarity, 100% high osmolarity and the point at which the proportion of each is 50%. Interpolation between these three points allows for any ratio to be obtained. By carefully controlling the hydrostatic pressure difference, the total hydrostatic pressure of the center channel can be controlled, ensuring a constant flow rate despite differing concentration ratios.

To ensure proper mixing of the resulting fluid from the W-junction, a mixing layer was added to the design of the chip. This secondary layer spans the length of the channel prior to combining with the red blood cell suspension and works to create turbulence in order to thoroughly combine the low and high osmolarity solutions. A mixing layer for the red blood cell suspension and the final salt solution was deemed unnecessary as the presence of cells causes enough disruption in normal laminar flow around the boundaries to ensure proper mixing.

Silicon mold production

The silicon mold for the microchips was created with photolithography using a mask produced by ink printing on transparent plastic according to the specifications in Figure 3.1 The photomask was made using ink which has a limitation of the smallest feature size being 8 μm. In addition, the vertical limit on feature size meant that approximating a round cross section for the chip would be impossible without increasing the number of layers and the diameter of the channel.

Thus, the main channel on the chip which is meant to approximate microcirculatory flow has a square cross section. The difference for flow between a circular and square cross section is most pronounced closest to the boundary layer. However, the flow in the center of a square cross section is a good approximation of a circular cross section.

The silicon mold was manufactured as a set of 16 identical chips. Minor manufacturing errors make it necessary to treat these as similar instead of identical. Several chips were noted as faulty during use and subsequent chips from those sections of the mold were consistently discarded after each production cycle. Additionally, some chips provided a different flow rate in the main channel for the same applied hydrostatic pressure likely due to a combination of small channel defects and variance in port construction. Thus, initially, the presence of fluorescent beads and later, the red blood cells themselves served as a way to control for flow speed within the channel instead of relying on the exact hydrostatic pressures. Once working chips were found, they were identified by serial number imprinted in the PDMS and chips from the same location on the mold were used in subsequent batches. This was necessary to reduce any errors resulting from individual chip differences from the mold.

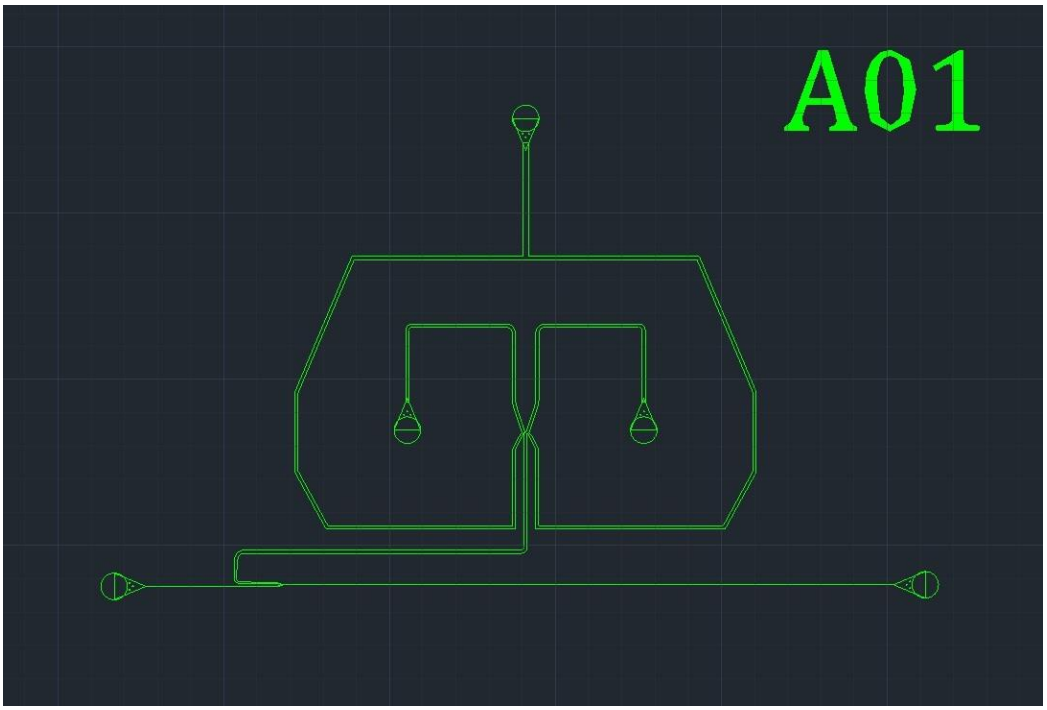

Figure 3.1 CAD diagram of the main layer of the first microchip (A01) out of a total of 16 (A16). Circle indicate locations for inlets or outlets. Bottom-right and top outlets are for waste. Bottom-left serves as the main inlet for red blood cell suspension. The two center inlets feed into the W-junction in the center of the chip. Minimum feature size for this design was 8 um.

PDMS chip manufacturing

Using aluminum foil to create height, PDMS was poured directly on top of the silicon wafer. Because PDMS is made as a mixture of two components which need to be vigorously stirred together prior to use, the entire mold remained in a vacuum chamber until air pockets were fully removed. Following this, the PDMS was hardened in an oven, baking at 80 °C for 1 hour. Solid PDMS was removed for the silicon wafer taking care to avoid damaging the mold. Individual chips were cut from the PDMS and ports are punched using a 26 gauge leur stub. Completed ports were cleaned with deionized water to ensure the port has a proper exit and remove small pieces of PDMS which might otherwise block the channels. PDMS chips were cleaned with 70% ethanol and deionized water while each corresponding glass coverslip is cleaned with sequential washings of n-heptane, methanol, and deionized water. Both chip and coverslip were placed in an ultraviolet ozone cleaner for 3 minutes to activate the surfaces. Following ozone treatment, chips were each placed on a glass coverslip and gently pressed to allow the surfaces to bond.

Blood collection

Large quantities of blood were necessary to achieve a 20% hematocrit in the main channel of the chip. Wild-type and AQP1 knockout mice blood was collected by heart puncture following cervical dislocation. This method provided enough blood when diluted to 20% hematocrit in order to fill a 50 mL syringe to the minimum height necessary for a constant liquid surface area over the full duration of the experiment. Large syringes must be used as any significant change in liquid

height over the duration of the experiment would alter the speed of blood flow within the channel.

SYTOX green was chosen to be the fluorescent reporter for the red blood cell surroundings. This dye is a commonly used viability stain and as such is both impermeable to the erythrocyte membrane as well as non-toxic to living cells. Because SYTOX green exhibits very low fluorescence when not in the presence of its binding target, nucleic acids, a high concentration of 50 μM was used. Because the containing-junction channel would vary in the combined ratio of high and low osmolarity inputs, the dye was added to the erythrocyte suspension to reduce the complexity of accounting for mixing ratio and to help ensure a consistent initial concentration of the fluorophore.

Chip preparation for experimental use

Immediately before use, the channels of each chip were exposed to a solution of 1% bovine serum albumin (BSA) for 30 minutes in order to coat the PDMS and reduce red blood cell adhesion to the channel walls. Any adhesion of the red blood cells would lead to a change in the resistance of the channel, requiring a change in pressure to achieve the desired flow rate, as well as potentially causing a full blockage of the channel over time. Each chip was placed in a vacuum chamber for 45 minutes to remove air from the channels and facilitate the addition of the BSA solution without creating air pockets. BSA was run through 26 gauge Tygon tubing and connected to the chip with a blunt 26 gauge needle bent at a 90 degree angle as detailed in [Voigt, C. 2011].

Five 50 mL syringes per chip were prepared with blunt 26 gauge needles connected to 6 feet of Tygon tubing. Each working solution (two salt solutions, red

blood cell suspension, and two waste solutions composed of deionized water) was placed in their respective syringe and the fluid was allowed to flow the entire length of the tubing until consistent flow was established to prevent air pockets from entering the chip. Immediately prior to imaging, the tubing is connected to the chip with blunt 26 gauge needles and the syringes are set at the desired height to generate hydrostatic pressure necessary for flow. Absolute heights varied between each chip due to differences in manufacturing with the relative fluid levels remaining mostly consistent. The red blood cell suspension was placed 4 cm higher than the height for a 50% ratio between the two salt solutions and the waste solutions were placed 10 cm below the red blood cell suspension. Because each chip could respond to hydrostatic pressure differently red blood cell speed was measured prior to and after mixing to obtain flow rates. Hydrostatic pressures were adjusted accordingly to obtain consistent flow conditions and mixing.

Imaging occurred on a Nikon fluorescent microscope using the exact set up and equipment described in chapter 14 of Synthetic Biology: Methods for part/device characterization and chassis engineering [Voigt, C., 2011]. Brightfield video was obtained using both 20 ms and 10 ms intervals while fluorescent video was imaged at 530 nm and was taken with both 10 ms and 100 ms intervals. Low speed video was best used to average fluorescent signal changes over longer time periods while high speed video was used to determine cell morphology and cell speed.

Brightfield measurements

Measurements of erythrocyte morphology averaged from brightfield video was used to estimate red blood cell volume changes at a position 60 μm

downstream from the mixing point. Red blood cells in the channel are observed to be randomly tumbling and thus a measure of their visible diameter over enough frames gives a measure of the effective shape that would be obtained from ensemble averaging the red blood cell projection from 3D to 2D. With this red blood cell volume estimation, a corresponding change in plasma volume can be calculated on the basis that the flow speed immediately prior to the red blood cell is unchanged to that immediately after creating a closed system of only two components for this frame of reference. Plasma volume change allows for the calculation of the osmolarity at any given point in the channel away from the initial mixing point. This value would be quantification of the effect red blood cells have on their surroundings

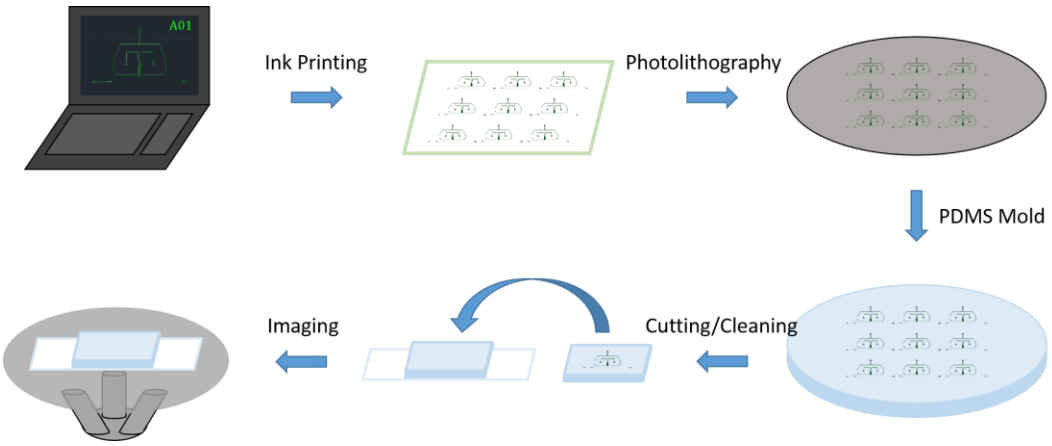

Figure 3.2 Overview of methodology used in the construction and use of a microfluidic device replicating capillary blood flow. Beginning with a computer designed schematic, a physical mold is built on top of a silicon wafer. PDMS is poured directly onto this surface to imprint the channels into the compound. Each PDMS chip is cut and bound to a glass coverslip using ozone to create closed channels.

Results

SYTOX green localization

Figure 3.3 shows red blood cells on a glass slide with SYTOX green. Red blood cells seen in brightfield appeared as regions with no fluorescent signal when reading emissions from 530 nm. Establishing the localization of the fluorescent reporter was both important to dye selection as well as viability of use in the microfluidic chip. Additionally, the dye intensity from these results was used to establish the final working dye concentration to be used in the device.

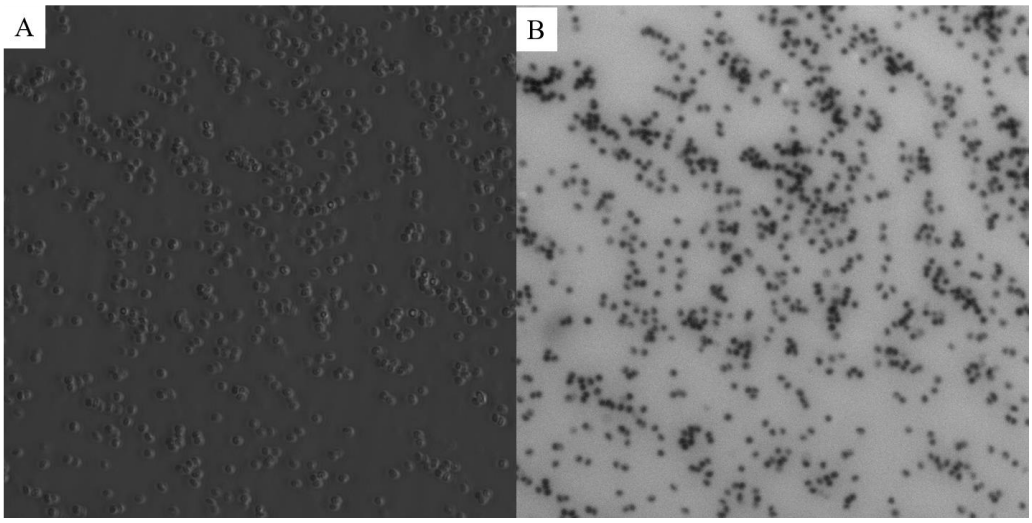

Figure 3.3 Brightfield and fluorescent images of red blood cells with SYTOX green. Comparison of brightfield (A) and fluorescent (B) images shows the complete non-localization of the dye with the red blood cells. SYTOX green is non-permeable to living red blood cells.

Brightfield videomicroscopy

Brightfield results taken of the 10 μm x 10 μm cross section channel show the ability of this device to handle red blood cell suspensions of 20% hematocrit with no difficulty. Coating the channel walls with BSA extends the usable lifetime of the microchip by preventing cell adhesion to the walls of the channel. Additionally, the red blood cell suspension flows through a simple channel with only a single bifurcation. These factors combined allow for a high hematocrit suspension to be used in a PDMS device with narrow channels.

Figure 3.4 shows the mixing point between the red blood cell suspension and salt solution. The design of the W-junction previously seen in Figure 3.1 allows the osmolarity of the salt solution to be changed without physically disconnecting anything from the microchip. This enables flow conditions to remain constant when changing the osmolarity for different test conditions.

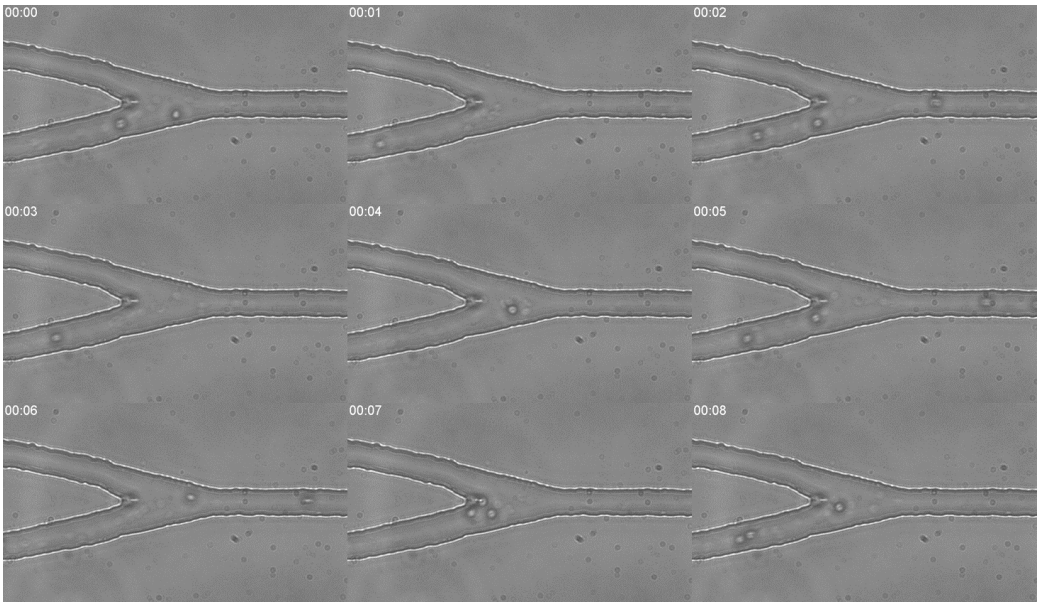

Figure 3.4 Brightfield timelapse of red blood cell suspension mixing with salt solution. Channel depth of 10 μm allows for some red blood cells to be in focus while others appear out of focus in the background. Red blood cell suspension is at 20% hematocrit and requires that channels are coated with BSA to prevent cell adhesion to the channel walls. Red blood cell suspension originates from lower channel and flows to the right. Salt solution originates from the upper channel and flows to the right. The number on the upper left corner of each frame indicates the time in seconds.

Flow speed of the red blood cell suspension is measured before and after mixing with salt solution using brightfield video (Figure 3.5). Consistency of flow speed between different conditions of osmolarity is necessary for accurate comparisons to be made. The 1.8mm/s speed of blood flow within the channel is on the high end for capillary blood flow (0.3 mm/sec-2 mm/sec) but is necessary to overcome the high resistance of the channel and to ensure blood clumps do not develop within the tubing before entering the narrow channels of the device where a blockage could form.

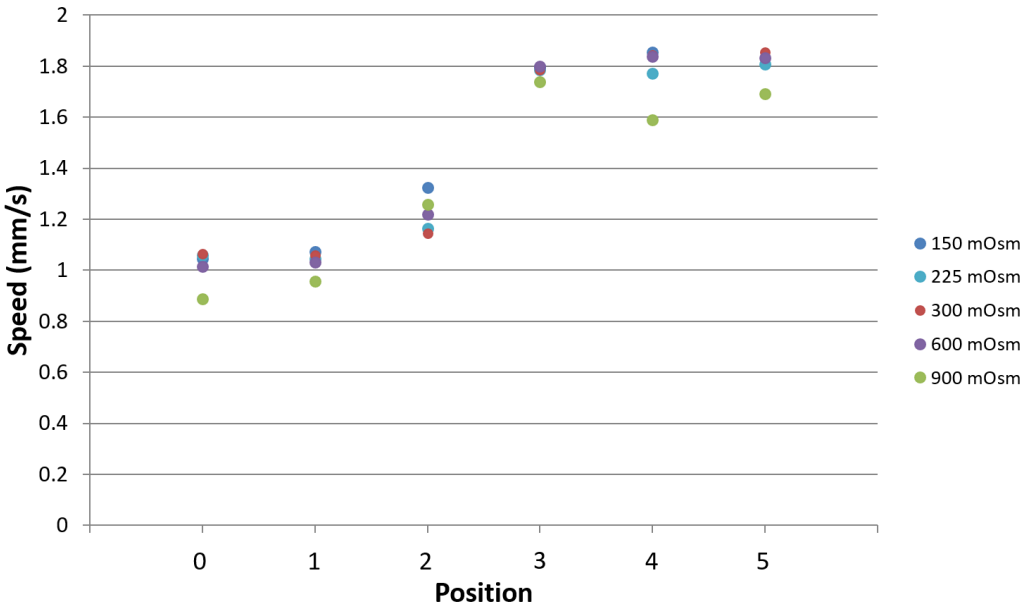

Figure 3.5 Change in speed occurring at mixing point between red blood cell suspension and salt solution. Combined channels caused an increase in pressure and flow speed in the final channel. Speed was measured from the position of visible red blood cells and was used to calculate the exact ratio at which the two channels are mixing.

Changes in SYTOX green intensity due to the presence of RBC

The fluorescent reporter SYTOX green, is used to identify changes in the surroundings of the red blood cells. Figure 3.6 demonstrates the absence of laminar flow at the mixing point of the red blood cell suspension and the salt solution. This is indicative of turbulent flows and is critical for the immediate mixing of the two channels. In order to establish that changes in fluorescent intensity are due to red blood cells, spectrophotometer data was obtained with SYTOX green and sodium chloride in concentrations corresponding to experimental conditions. Figure 3.7C shows the change in fluorescent intensity of SYTOX green with respect to changing salt concentrations. The slight increase in intensity is linear and is likely a result of salt interactions with the charged groups of SYTOX green. When combined with red blood cells, spectrophotometer readings show a different pattern of behavior. Comparison of Figure 3.7A and 3.7B shows the final measured points from the microfluidic chip match the behavior seen in the spectrophotometer readings. Given that the spectrophotometer reading are taken over the course of 20 minutes while the microfluidic chip final readings take place 60 ms after the mixing point, this likely indicates that the system reaches steady state after approximately 60 ms.

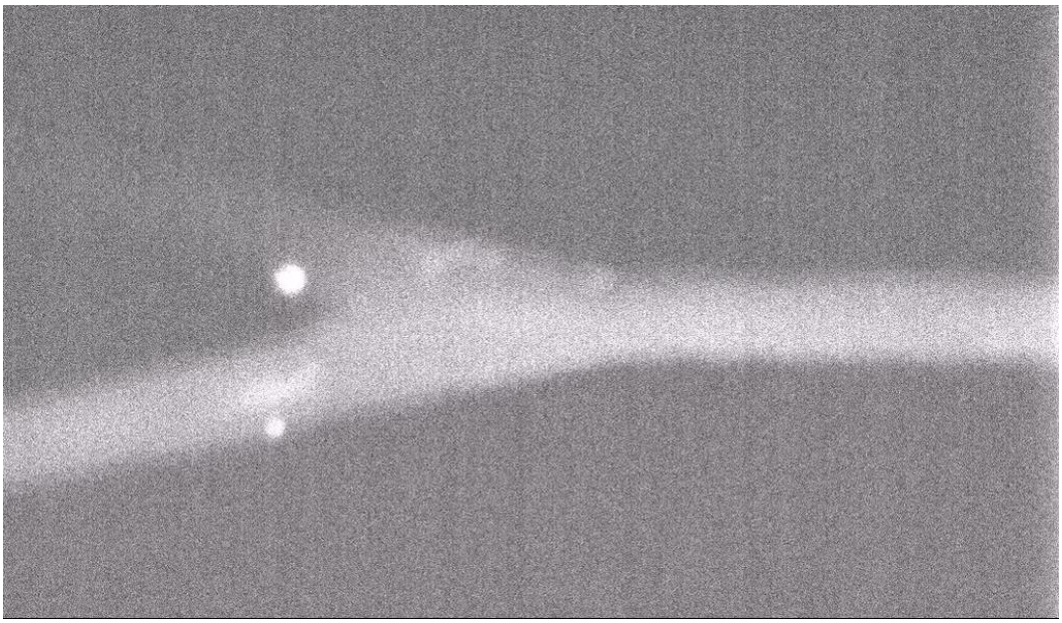

Figure 3.6 Fluorescent signal from SYTOX green at the mixing point between the red blood cell suspension and salt solution. Red blood cell suspension (bottom channel) mixes with salt solution (top channel). This image captured at 100 ms speed shows the averaged signal obtained from the channel. No red blood cells are visible using fluorescence.

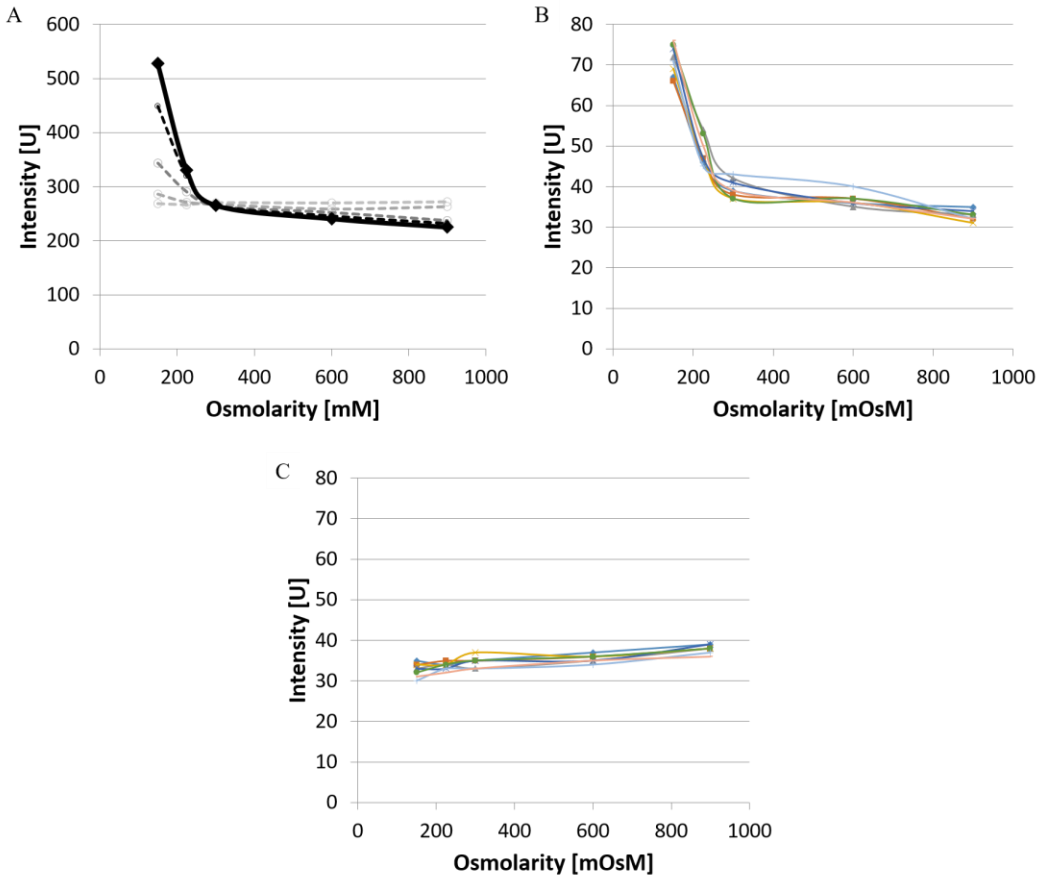

Figure 3.7 SYTOX green intensity measurements from microfluidic device compared to spectrophotometer measurements. (A) Intensity measurements for different salt concentrations. Dotted lines indicate positions closer to the mixing point of red blood cell suspension and salt solution while solid line represents measured point farthest from mixing point. (B) Spectrophotometer data taken from represented mixtures of red blood cells, NaCl, and SYTOX green in equal proportions to microfluidic device. (C) Spectrophotometer data of SYTOX green and NaCl without red blood cell suspension.

Figure 3.8 shows the change in intensity of SYTOX green at points along the microchip channel where each curve represents a different initial mixing osmolarity. The changes in fluorescent intensity reach steady state within the channel 60 ms after the red blood cell suspension mixes with the salt solution. Comparison of wild-type and AQP1 knockout red blood cells reveals a difference in the magnitude of changes. Fluorescent intensity changes are minor with AQP1 knockout red blood cells but still follow the trend established by the wild-type. In general, large intensity increases are seen for hypo osmotic conditions whereas smaller decreases in intensity are observed for hyperosmotic conditions. It is unclear whether these changes are due solely to red blood cell volume change or if potential effects from lysis or light scattering also play a role.

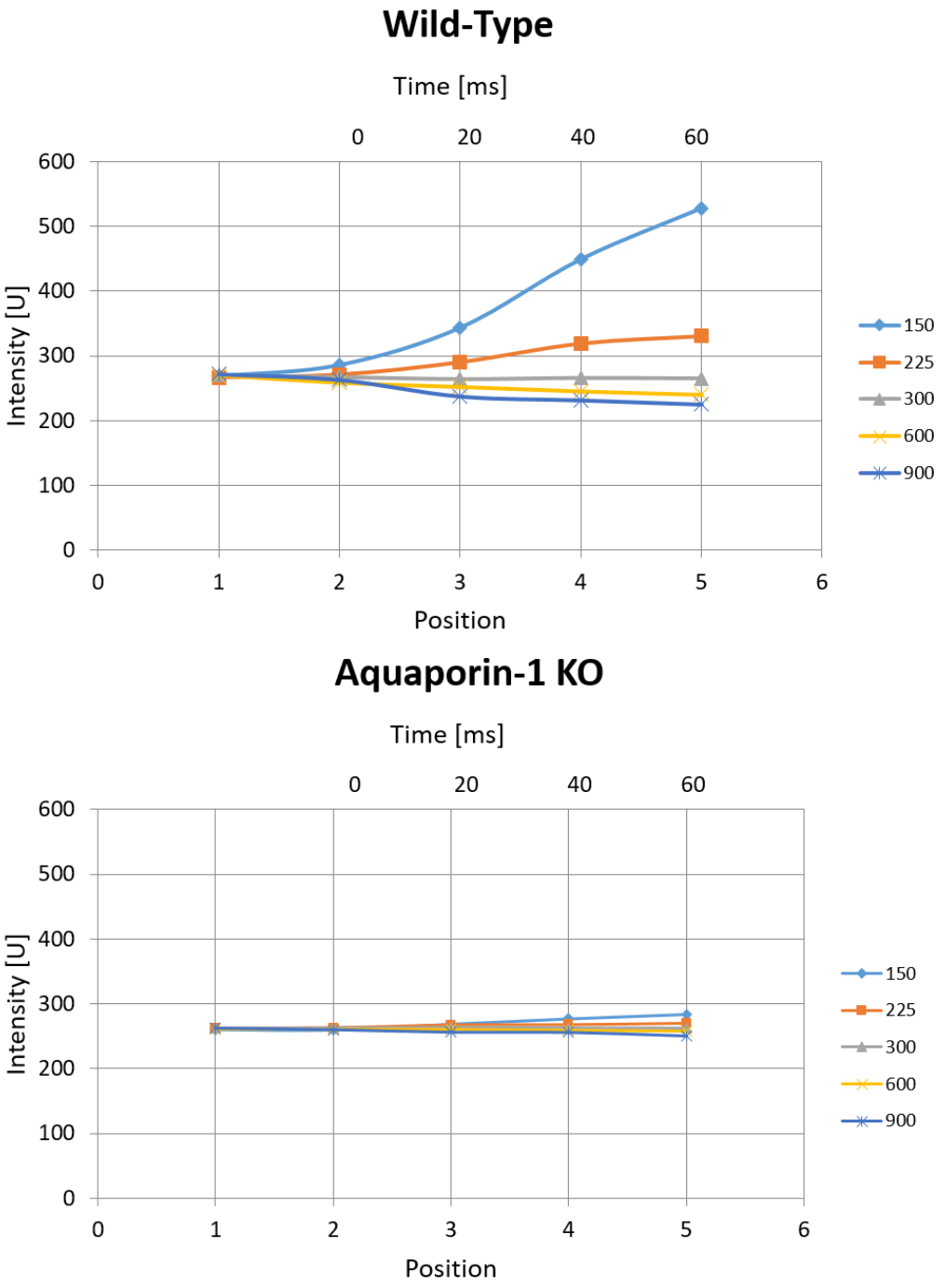

Figure 3.8 SYTOX green intensity from microfluidic device comparing wild-type to AQP1 knockout red blood cell suspensions. Intensity of SYTOX green changes over time. Each curve represents a different initial salt concentration. Changes to intensity are minimal with AQP1 red blood cell suspensions.

Brightfield estimations of red blood cell volume changes

Since channel geometry and hematocrit are known, the results of red blood cell volume change can be translated to “plasma” volume change for this pseudo-closed system under the assumption of constant flow speed. Plasma volume change is used to calculate the change in osmolarity due to red blood cells.

Figure 3.9 shows the estimates of red blood cell volume and corresponding changes to plasma volume estimated from brightfield videomicroscopy. Calculation of plasma volume assumes a closed system causing changes in red blood cell volume to be mirrored in the surrounding fluid. Figure 3.10 compares the changes seen in wild-type red blood cells to that from the AQP1 knockouts. Similar to results from chapters 1 and 2, the AQP1 knockout displays little volume change. However, the wild-type red blood cells exhibit a larger volume change than was previously observed in the hyperosmotic conditions. This is likely caused by the nature of the volume estimation and places importance on the need for the more accurate volume measurement previously used in Chapter 1.

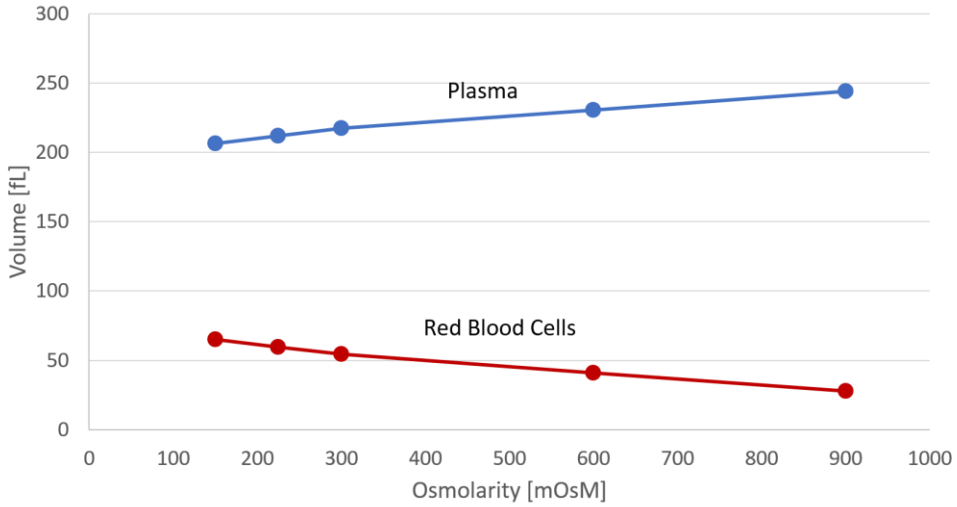

Figure 3.9 Brightfield estimations of red blood cell volume changes and corresponding plasma volume changes. Red blood cell volumes estimated from brightfield video measurements for different salt concentrations taken 60 ms after mixing point. Any change to red blood cell volume should be mirrored in the plasma volume for this pseudo-closed system.

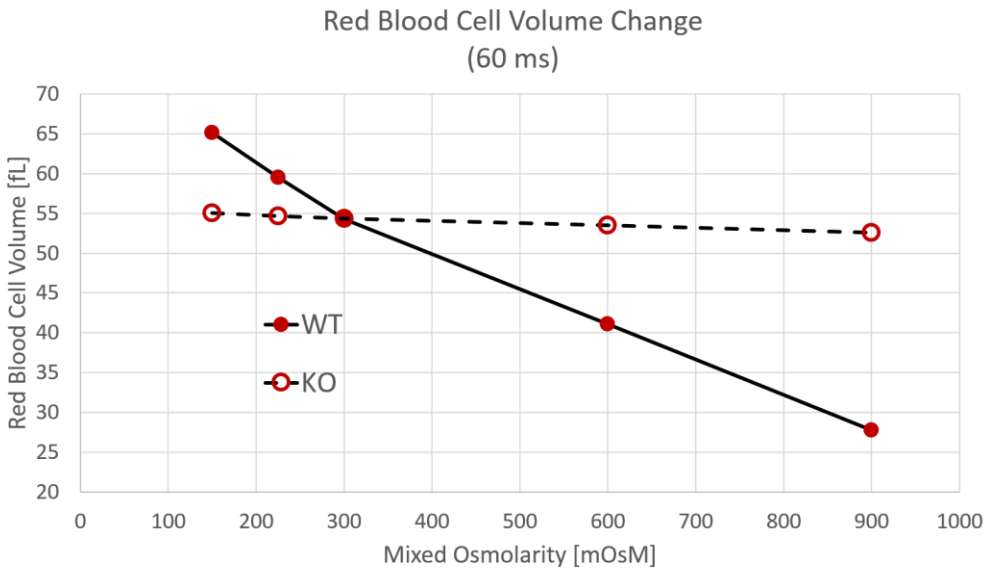

Figure 4.10 Red blood cell volume change estimated from brightfield videomicroscopy for wild-type and AQP1 knockout red blood cells. Similar to previous results from chapters 1 and 2, wild-type red blood cells experience a large volume change relative to AQP1 knockout for the same osmotic pressures. Larger volume change is observed here compared with previous results and is likely due to the nature of the volume estimation.

The magnitude of changes due to red blood cells can be seen in Figure 3.11. Maximum change in osmolarity can be seen with the highest initial mixing osmolarity while minimum change can be seen at the lowest initial mixing osmolarity. The behavior of osmolarity changes around the iso-osmolarity point of 300 mOsM can be approximated as linear. For the range 290 mOsM to 310 mOsM the magnitude of the red blood cell effect is approximately 20%. Thus, for small changes to plasma osmolarity, red blood cells can provide a buffer effect that reduces these changes by 20%. In the range of high salt concentration, this buffer effect is reduced to approximately 17%.

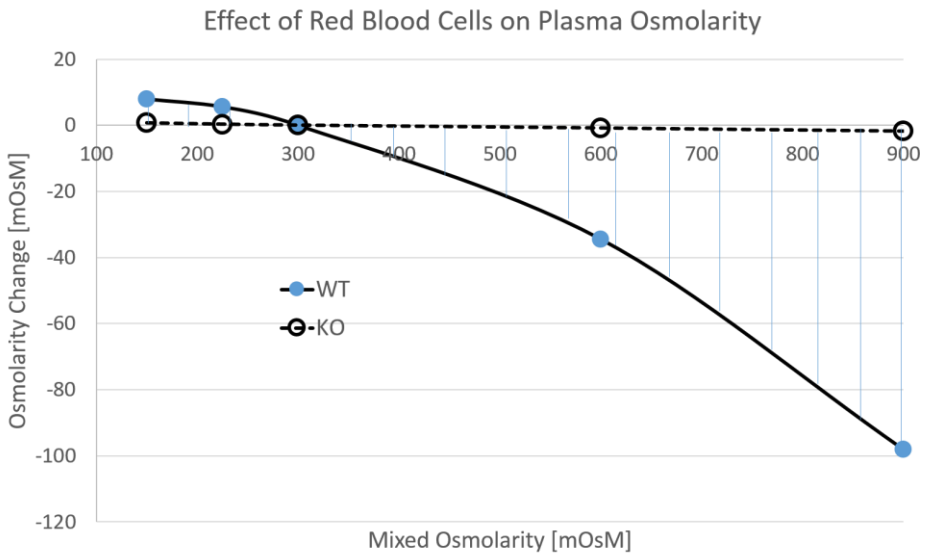

Figure 3.11 Change in plasma osmolarity due to red blood cell volume change. Water transport from red blood cells changes osmolarity in the surrounding fluid. Considering possible changes from iso osmolarity (300 mOsM) the effect red blood cells provide is a buffer from 17 to 20%. For example, changing from 300 to 310 mOsM causes a reduction by blood cells to plasma osmolarity of 308 (310-308/10 = 20%).

Discussion

Microfluidic chip design

The versatility of PDMS microchips also has some disadvantages. Specifically, the mass production of the chips means that slight variations between chips exist. While individual defects were not immediately apparent on visual inspection of each chip, differences most commonly manifested in the relation between hydrostatic pressure and flow speed in certain channels of the chip. Thus it was necessary to control the flow speed within the channels of the chip as opposed to the hydrostatic pressure of the inlets and outlets in order to ensure consistent measurements. Additionally, slight deviations of temperature or mixing rates of the PDMS are able to cause total chip failures. The particular point of greatest stress for the microfluidic chip is the ports. While the majority of the chip is sealed to glass by chemical bonding, the ports are sealed by the friction between the 26 gauge stub and the PDMS walls. Combined with the high hydrostatic pressures necessary to drive the flow within these microchips, small defects to the walls here can rupture causing loss of pressure within the chip leading to complete mechanical failure. Faulty connections like this were the primary cause for microchip failure and highlight the need for mass production. Non-disposable chips typically have built in connectors which rely on mechanical hinges as opposed to friction for their ports. Unfortunately, this type of solution is too impractical for disposable chips with ports made by hand.

Ideally a channel with a circular cross section would be used to replicate capillary flow. However, producing a round cross section using photolithography is both challenging and would produce less than ideal results. The process of creating a round cross section would require multiple, thin layers of PDMS to

approximate a smooth, rounded surface. Unlike a rectangular channel which can be a single layer, the mold for a round channel would need to be divided into multiple sections and the final result put together in a single chip during the manufacturing and manipulation of the PDMS. These errors that are likely to accumulate from this process are avoided entirely with the use of a square channel which closely approximates the flow pattern seen in a circular cross section channel. The flow is most similar in the center of the channel which is the location that most red blood cells will move in. Because of this, a square channel was deemed the better option when considering the design of the chip.

Fluorescent intensity with RBC suspensions

Intensity measurements taken from the epifluorescent microscope present a unique challenge. Red blood cells in solution contribute to a significant amount of light scattering and absorption. Additionally, the use of SYTOX green means that even picogram amounts of RNA are able to affect intensity readings. Because of this, attempts at connecting red blood cell size directly to fluorescent intensity were not feasible at this time due to complications from light scattering and potential cell lysis. Instead, changes to fluorescence are best used to measure the timescale of the changes that occur. Because no laminar flow was observed at the mixing point (see Figure 3.6), it can be assumed that the channel is well mixed.

Comparison of wild-type and AQP1 knockout red blood cells

Compared to *in vivo* results, the comparison between wild-type and AQP1 knockout *in vitro* can more accurately reveal the role of AQP1 in the erythrocyte membrane. By isolating the red blood cells, the role that AQP1 plays in other

tissues throughout the body is no longer relevant. The tests here imply water transport reduced by an order of magnitude between wild-type and AQP1 knockout. In the perspective of locality, this suggests that a red blood cell without AQP1 would be unable to fully respond to a local stimulus without traveling approximately 600 μm as opposed to 60 μm. This shows that the presence of AQP1 is a necessary factor for red blood cells to respond to osmotic pressure in their immediate vicinity.

The volume change results seen here are mostly consistent with the change observed *in vivo*, but differ slightly in magnitude. Specifically, a larger volume decrease is measured in response to less osmotic pressure than is assumed to be present in the kidney. Similar to difficulties in chapter 1, this is likely to be caused by inaccuracies in the method of volume estimation due to the complex shape of the crenated red blood cell. It is not unreasonable to think that the protruding spikes created when crenated are not able to be accounted for in a bulk averaging method from video frames 10 ms apart. This would make all estimations of red blood cell volume smaller than they should be for hyperosmotic conditions.

Chapter 3, in part is currently being prepared for submission for publication of the material. Sugie, Joseph; Sung, L. Amy. The dissertation author was the primary investigator and author of this material.

.

CONCLUSIONS

Combining experimental results and theoretical analysis from Chapters 1, 2 and 3 leads to a greater understanding of red blood cells as regulators of water balance. Newly developed negative imaging techniques in combination with confocal microscopy enabled large scale data collection and measurement necessary to investigate red blood cell volume distributions in both wild-type and AQP1 knockout kidneys. These results revealed up to a 40% decrease in red blood cell volume against the hyperosmotic gradient in the medulla of the kidney. Simulations of these capillaries were in agreement with experimental results. Analysis revealed the possibility that red blood cells may function as micropumps to facilitate the water transport among cells, plasma, and interstitial space. Additionally, the simulations revealed the functional role of red blood cells in vasa recta in maintaining the hyperosmotic gradient critical to the concentration and production of urine. Microfluid studies showed a 60 ms time to reach steady state and indicated that the presence of red blood cells provides a buffer to changes in plasma osmolarity as great as 20%.

Using conventional estimates, the average human has 20 trillion red blood cells in their blood, each containing 200,000 copies of AQP1[King et al., 2000]. Unlike other means of water balance in the body such as excretion of urine, exhale of water vapor, shedding of tears, and uptake of water from drinks and food, that occur at given specific tissue or organ, regulation due to red blood cells is omnipresent throughout. Assuming 5L of blood in the body, red blood cells are altogether capable of moving close to a full liter of water. This volume of water is a significant amount, comparable to that lost through urine over a 24 hour period.

Hormonal regulation of water balance is primarily accomplished through the action of anti-diuretic hormone (ADH) also known as arginine vasopressin

(AVP). Secretion of ADH occurs via sensing of plasma osmolarity by cells termed osmoreceptors [Harris, H.W. et al., 1991]. As their name suggests, these cells expand and contract in response to changes in plasma osmotic pressure and send signals to the hypothalamus triggering the release of ADH from the pituitary where it is stored. Osmotic sensing is sensitive to changes as small as 1 mOsM which are observed to cause direct increases to plasma ADH [Verbalis, J.G. 2003]. This circulating ADH works to reabsorb water from the collecting duct of the kidney by moving aquaporin-2 from the cytoplasm to the apical membrane in order to increase water permeability. Similar to ADH, aldosterone is a hormone involved in the renin-angiotensin-aldosterone system. Though this hormone has many different effects, secretion is modulated by plasma osmolarity and it affects reabsorption of water in the kidney through the movement of NaCl. Evidence indicates that these hormone, which affect water loss to urine through the kidneys are the primary method of active water regulation.

When investigating full body water balance and homeostasis, both passive and active methods of regulation must be considered. Passive water transport from red blood cells provides a buffer, able to reduce high osmolarity by 20% for osmolarity toward iso osmolar according to microfluidic data. Red blood cells can be found throughout the whole body and can respond to concentration gradients quick enough to affect the local osmolarity. Additionally, this form of regulation by red blood cells requires no energy expenditure.

Because ADH and aldosterone, both hormones that regulate water, respond to changes in plasma osmolarity they are affected by the passive regulation resulting from the presence of red blood cells. ADH in particular is sensitive enough that this passive buffer effect will cause significant changes to

the hormone's plasma concentration. In fact the sensitivity of ADH itself implies a need for passive regulation, without which concentration of this hormone may fluctuate wildly given small changes in plasma osmolarity.

In summary, examination of the ability of red blood cells to respond to osmotic gradients *in vivo* and the significance of this response on their surroundings suggests that red blood cells provide important regulation of water balance and homeostasis. Thus we conclude that, in addition to O_2 and CO_2 gas exchange, water transport and homeostasis may well be the third major function of red blood cells.

REFERENCES

Benga, G. (1988). Water transport red blood cell membranes. Progress in Biophysics and Molecular Biology *51*, 193–245.

Benga, G. (2012). The first discovered water channel protein, later called aquaporin 1: Molecular characteristics, functions and medical implications. Molecular Aspects of Medicine *33*, 518–534.

Blanc, L., Liu, J., Vidal, M., Chasis, J.A., An, X., and Mohandas, N. (2009). The water channel aquaporin-1 partitions into exosomes during reticulocyte maturation: implication for the regulation of cell volume. Blood *114*, 3928–3934.

Borgnia, M., Nielsen, S., Engel, A., and Agre, P. (1999). Cellular and Molecular Biology of the Aquaporin Water Channels. Annual Review of Biochemistry *68*, 425–458.

Bow, H.C. (2010). Microfluidic devices for analysis of red blood cell mechanical properties. Thesis. Massachusetts Institute of Technology.

Brahm, J. (1983). Kinetics of glucose transport in human erythrocytes. The Journal of Physiology *339*, 339–354.

Carbrey, J.M., and Agre, P. (2009). Discovery of the Aquaporins and Development of the Field. In Aquaporins, P.D.E. Beitz, ed. (Springer Berlin Heidelberg), pp. 3–28.

Chen, J., Layton, A.T., and Edwards, A. (2009). A mathematical model of O2 transport in the rat outer medulla. I. Model formulation and baseline results. American Journal of Physiology - Renal Physiology *297*, F517–F536.

Chen, J., Edwards, A., and Layton, A.T. (2010). Effects of pH and medullary blood flow on oxygen transport and sodium reabsorption in the rat outer medulla. American Journal of Physiology - Renal Physiology *298*, F1369–F1383.

Chou, C.-L., Knepper, M.A., Hoek, A.N. van, Brown, D., Yang, B., Ma, T., and Verkman, A.S. (1999). Reduced water permeability and altered ultrastructure in thin descending limb of Henle in aquaporin-1 null mice. J Clin Invest *103*, 491–496.

Costa, M., Ghiran, I., Peng, C.-K., Nicholson-Weller, A., and Goldberger, A.L. (2008). Complex dynamics of human red blood cell flickering: Alterations with \textit{in vivo} aging. Phys. Rev. E *78*, 020901.

Effros, R.M., Darin, C., Jacobs, E.R., Rogers, R.A., Krenz, G., and Schneeberger, E.E. (1997). Water transport and the distribution of aquaporin-1 in pulmonary air spaces. Journal of Applied Physiology *83*, 1002–1016.

Esteva-Font, C., Ballarin, J., and Fernández-Llama, P. (2011). Molecular biology of water and salt regulation in the kidney. Cell. Mol. Life Sci. *69*, 683–695.

Evans, E.A., Waugh, R., and Melnik, L. (1976). Elastic area compressibility

modulus of red cell membrane. Biophys J *16*, 585–595.

Farinas, J., and Verkman, A.S. (1996). Cell volume and plasma membrane osmotic water permeability in epithelial cell layers measured by interferometry. Biophys J *71*, 3511–3522.

Fedosov, D.A., Caswell, B., Popel, A.S., and Karniadakis, G.E. (2010). Blood Flow and Cell-Free Layer in Microvessels. Microcirculation *17*, 615–628.

Fenton, B.M., Carr, R.T., and Cokelet, G.R. (1985). Nonuniform red cell distribution in 20 to 100 μm bifurcations. Microvascular Research *29*, 103–126.

Friebel, M., Helfmann, J., Netz, U., and Meinke, M. (2009). Influence of oxygen saturation on the optical scattering properties of human red blood cells in the spectral range 250to2000nm. J. Biomed. Opt *14*, 034001–034001 – 6.

Funder, J., and Wieth, J.O. (1976). Chloride transport in human erythrocytes and ghosts: a quantitative comparison. The Journal of Physiology *262*, 679–698.

Fung, Y.-C. (1973). Stochastic flow in capillary blood vessels. Microvascular Research *5*, 34–48.

Gottschalk, C.W., and Mylle, M. (1958). Evidence that the mammalian nephron functions as a countercurrent multiplier system. Science *128*, 594.

Gottschalk, C.W., and Mylle, M. (1959). Micropuncture study of the mammalian urinary concentrating mechanism: evidence for the countercurrent hypothesis. American Journal of Physiology -- Legacy Content *196*, 927–936.

Grimberg, B.T., Scheetz, E.A., Erickson, J.J., Bales, J.M., David, M., Daum-Woods, K., King, C.L., and Zimmerman, P.A. (2012). Increased reticulocyte count from cord blood samples using hypotonic lysis. Experimental Parasitology *132*, 304–307.

Ham, T.H., Dunn, R.F., Sayre, R.W., and Murphy, J.R. (1968). Physical Properties of Red Cells as Related to Effects in Vivo. I. Increased Rigidity of Erythrocytes as Measured by Viscosity of Cells Altered by Chemical Fixation, Sickling and Hypertonicity. Blood *32*, 847–861.

Hammer, M., Schweitzer, D., Michel, B., Thamm, E., and Kolb, A. (1998). Single Scattering by Red Blood Cells. Applied Optics *37*, 7410.

Harris, H.W., Strange, K., and Zeidel, M.L. (1991). Current understanding of the cellular biology and molecular structure of the antidiuretic hormone-stimulated water transport pathway. J Clin Invest *88*, 1–8.

Hochmuth, R.M., and Waugh, R.E. (1987). Erythrocyte Membrane Elasticity and Viscosity. Annual Review of Physiology *49*, 209–219.

Holliger, C., Lemley, K.V., Schmitt, S.L., Thomas, F.C., Robertson, C.R., and

Jamison, R.L. (1983). Direct determination of vasa recta blood flow in the rat renal papilla. Circulation Research *53*, 401–413.

Jay, A.W.L., and Burton, A.C. (1969). Direct Measurement of Potential Difference across the Human Red Blood Cell Membrane. Biophys J *9*, 115–121.

Jelkmann, W. (1992). Erythropoietin: structure, control of production, and function. Physiological Reviews *72*, 449–489.

Jelkmann, W. (2007). Erythropoietin after a century of research: younger than ever. European Journal of Haematology *78*, 183–205.

Johnson, A.E., Le, I.P., Andresen, B.T., Stodola, J., Dewey, G.L., Dean, S.B., Resau, J., Haak, P., Ruch, T., Sartor, A., et al. (2012). VACM-1/cul5 expression in vascular tissue in vivo is induced by water deprivation and its expression in vitro regulates aquaporin-1 concentrations. Cell Tissue Res *349*, 527–539.

King, L.S., Yasui, M., and Agre, P. (2000). Aquaporins in health and disease. Molecular Medicine Today *6*, 60–65.

Kleinhans, F.W. (1998). Membrane Permeability Modeling: Kedem–Katchalsky vs a Two-Parameter Formalism. Cryobiology *37*, 271–289.

Kokko, J.P., and Rector, F.C. (1972). Countercurrent multiplication system without active transport in inner medulla. Kidney Int. *2*, 214–223.

Kosinska Eriksson, U., Fischer, G., Friemann, R., Enkavi, G., Tajkhorshid, E., and Neutze, R. (2013). Subangstrom resolution X-ray structure details aquaporin-water interactions. Science *340*, 1346–1349.

Kuchel, P.W., and Benga, G. (2005). Why does the mammalian red blood cell have aquaporins? Biosystems *82*, 189–196.

Layton, A.T. (2007). Role of UTB Urea Transporters in the Urine Concentrating Mechanism of the Rat Kidney. Bull. Math. Biol. *69*, 887–929.

Layton, A.T., and Layton, H.E. (2005). A region-based mathematical model of the urine concentrating mechanism in the rat outer medulla. I. Formulation and base-case results. American Journal of Physiology - Renal Physiology *289*, F1346–F1366.

Layton, A.T., and Layton, H.E. (2011). Countercurrent multiplication may not explain the axial osmolality gradient in the outer medulla of the rat kidney. American Journal of Physiology - Renal Physiology *301*, F1047–F1056.

Layton, A.T., Pannabecker, T.L., Dantzler, W.H., and Layton, H.E. (2004). Two modes for concentrating urine in rat inner medulla. American Journal of Physiology - Renal Physiology *287*, F816–F839.

Lenormand, G., Hénon, S., Richert, A., Siméon, J., and Gallet, F. (2001). Direct

Measurement of the Area Expansion and Shear Moduli of the Human Red Blood Cell Membrane Skeleton. Biophysical Journal *81*, 43–56.

Ma, T., and Verkman, A.S. (1999). Aquaporin water channels in gastrointestinal physiology. The Journal of Physiology *517*, 317–326.

Ma, T., Yang, B., Gillespie, A., Carlson, E.J., Epstein, C.J., and Verkman, A.S. (1998). Severely impaired urinary concentrating ability in transgenic mice lacking aquaporin-1 water channels. J. Biol. Chem. *273*, 4296–4299.

Macey, R.I. (1984). Transport of water and urea in red blood cells. American Journal of Physiology - Cell Physiology *246*, C195–C203.

Macey, R.I., and Yousef, L.W. (1988). Osmotic stability of red cells in renal circulation requires rapid urea transport. American Journal of Physiology - Cell Physiology *254*, C669–C674.

Marieb, E.N., and Hoehn, K. (2013). Human anatomy & physiology (Boston: Pearson).

Mun, G.I., Jang, S.I., and Boo, Y.C. (2013). Laminar shear stress induces the expression of aquaporin 1 in endothelial cells involved in wound healing. Biochemical and Biophysical Research Communications *430*, 554–559.

Nagaraja, S., Kapela, A., and Tsoukias, N.M. (2012). Intercellular Communication in the Vascular Wall: A Modeling Perspective. Microcirculation *19*, 391–402.

Nielsen, S., Frøkiær, J., Marples, D., Kwon, T.-H., Agre, P., and Knepper, M.A. (2002). Aquaporins in the Kidney: From Molecules to Medicine. Physiological Reviews *82*, 205–244.

Nonoyama, A., Garcia-Lopez, A., Garcia-Rubio, L.H., Leparc, G.F., and Potter, R.L. (2011). Hypochromicity in red blood cells: an experimental and theoretical investigation. Biomedical Optics Express *2*, 2126.

Ottino, J.M., and Wiggins, S. (2004). Introduction: mixing in microfluidics. Philosophical Transactions of the Royal Society of London A: Mathematical, Physical and Engineering Sciences *362*, 923–935.

Overton, E. (1896). Über die osmotischen Eigenschaften der Zelle in ihrer Bedeutung für die Toxikologie und Pharmakologie. Z. Phys. Chem *22*, 189–209.

Pallone, T.L., Edwards, A., Ma, T., Silldorff, E.P., and Verkman, A.S. (2000). Requirement of aquaporin-1 for NaCl-driven water transport across descending vasa recta. J Clin Invest *105*, 215–222.

Pallone, T.L., Zhang, Z., and Rhinehart, K. (2003). Physiology of the renal medullary microcirculation. American Journal of Physiology - Renal Physiology *284*, F253–F266.

Preston, G.M., Carroll, T.P., Guggino, W.B., and Agre, P. (1992). Appearance of Water Channels in Xenopus Oocytes Expressing Red Cell CHIP28 Protein. Science *256*, 385–387.

Preston, G.M., Smith, B.L., Zeidel, M.L., Moulds, J.J., and Agre, P. (1994). Mutations in aquaporin-1 in phenotypically normal humans without functional CHIP water channels. Science *265*, 1585–1587.

Pries, A.R., Ley, K., Claassen, M., and Gaehtgens, P. (1989). Red cell distribution at microvascular bifurcations. Microvascular Research *38*, 81–101.

Rand, R.P., and Burton, A.C. (1964). Mechanical Properties of the Red Cell Membrane. Biophys J *4*, 115–135.

Renkin, E.M. (1977). Multiple pathways of capillary permeability. Circ. Res. *41*, 735–743.

Salathe, E.P., and An, K.-N. (1976). A mathematical analysis of fluid movement across capillary walls. Microvascular Research *11*, 1–23.

Schmid-Schönbein, G.W., Skalak, R., Usami, S., and Chien, S. (1980). Cell distribution in capillary networks. Microvascular Research *19*, 18–44.

Secomb, T.W., Skalak, R., Özkaya, N., and Gross, J.F. (1986). Flow of axisymmetric red blood cells in narrow capillaries. Journal of Fluid Mechanics *163*, 405–423.

Sierra, A. de la, Coca, A., Paré, J.C., Sánchez, M., Valls, V., and Urbano-Márquez, A. (1993). Erythrocyte ion fluxes in essential hypertensive patients with left ventricular hypertrophy. Circulation *88*, 1628–1633.

Steinke, J.M., and Shepherd, A.P. (1988). Comparison of Mie theory and the light scattering of red blood cells. Applied Optics *27*, 4027.

Strieter, J., Stephenson, J.L., Giebisch, G., and Weinstein, A.M. (1992). A mathematical model of the rabbit cortical collecting tubule. American Journal of Physiology - Renal Physiology *263*, F1063–F1075.

Sung, L.A., and Vera, C. (2003). Protofilament and Hexagon: A Three-Dimensional Mechanical Model for the Junctional Complex in the Erythrocyte Membrane Skeleton. Annals of Biomedical Engineering *31*, 1314–1326.

Thompson, T.E., and Huang, C. (1966). The Water Permeability of Lipid Bilayer Membranes*. Annals of the New York Academy of Sciences *137*, 740–744.

Tomaiuolo, G., Barra, M., Preziosi, V., Cassinese, A., Rotoli, B., and Guido, S. (2011). Microfluidics analysis of red blood cell membrane viscoelasticity. Lab Chip *11*, 449–454.

Toner, M., and Irimia, D. (2005). BLOOD-ON-A-CHIP. Annu Rev Biomed Eng *7*,

77–103.

Verbalis, J.G. (2003). Disorders of body water homeostasis. Best Practice & Research Clinical Endocrinology & Metabolism *17*, 471–503.

Verkman, A.S. (2005). More than just water channels: unexpected cellular roles of aquaporins. J Cell Sci *118*, 3225–3232.

Voigt, C. (2011). Synthetic Biology: Methods for part/device characterization and chassis engineering (Academic Press).

Walz, T., Hirai, T., Murata, K., Heymann, J.B., Mitsuoka, K., Fujiyoshi, Y., Smith, B.L., Agre, P., and Engel, A. (1997). The three-dimensional structure of aquaporin-1. Nature *387*, 624–627.

Williams, M.E. (2003). A review of reverse osmosis theory. EET Corporation and Williams Engineering Services Company, Inc.

Yang, B., Ma, T., and Verkman, A.S. (2001). Erythrocyte Water Permeability and Renal Function in Double Knockout Mice Lacking Aquaporin-1 and Aquaporin-3. J. Biol. Chem. *276*, 624–628.

Zimmerhackl, B., Dussel, R., and Steinhausen, M. (1985). Erythrocyte flow and dynamic hematocrit in the renal papilla of the rat. American Journal of Physiology - Renal Physiology *249*, F898–F902.